ASSESSMENT OF SINTERED WICK HEAT PIPE PERFORMANCE BY MODELING PHASE CHANGE IN SURFACE PORES

A THESIS SUBMITTED TO
THE GRADUATE SCHOOL OF NATURAL AND APPLIED SCIENCES
OF
MIDDLE EAST TECHNICAL UNIVERSITY

BY

ŞÜKRÜ KAAN YENER

IN PARTIAL FULFILLMENT OF THE REQUIREMENTS
FOR
THE DEGREE OF MASTER OF SCIENCE
IN
MECHANICAL ENGINEERING

APRIL 2024

Approval of the thesis:

ASSESSMENT OF SINTERED WICK HEAT PIPE PERFORMANCE BY MODELING PHASE CHANGE IN SURFACE PORES

submitted by **ŞÜKRÜ KAAN YENER** in partial fulfillment of the requirements for the degree of **Master of Science in Mechanical Engineering Department, Middle East Technical University** by,

Prof. Dr. Naci Emre Altun
Dean, Graduate School of **Natural and Applied Sciences** _____

Prof. Dr. M. A. Sahir Arıkan
Head of Department, **Mechanical Engineering** _____

Prof. Dr. Zafer Dursunkaya
Supervisor, **Mechanical Engineering, METU** _____

Assoc. Prof. Dr. Barbaros Çetin
Co-supervisor, **Mechanical Engineering, Bilkent University** _____

Examining Committee Members:

Assoc. Prof. Dr. Özgür Bayer
Mechanical Engineering, METU _____

Prof. Dr. Zafer Dursunkaya
Mechanical Engineering, METU _____

Assoc. Prof. Dr. Onur Taylan
Mechanical Engineering, METU _____

Assoc. Prof. Dr. Barbaros Çetin
Mechanical Engineering, Bilkent University _____

Assist. Prof. Dr. Alperen Günay
Mechanical Engineering, Bilkent University _____

Date:16.04.2024

I hereby declare that all information in this document has been obtained and presented in accordance with academic rules and ethical conduct. I also declare that, as required by these rules and conduct, I have fully cited and referenced all material and results that are not original to this work.

Name, Surname: Şükrü Kaan Yener

Signature :

ABSTRACT

ASSESSMENT OF SINTERED WICK HEAT PIPE PERFORMANCE BY MODELING PHASE CHANGE IN SURFACE PORES

Yener, Şükrü Kaan
M.S., Department of Mechanical Engineering
Supervisor: Prof. Dr. Zafer Dursunkaya
Co-Supervisor: Assoc. Prof. Dr. Barbaros Çetin

April 2024, 63 pages

With the advances in technology, managing thermal systems is becoming increasingly challenging. Due to their reliability, maintenance-free operation, and independence from external energy sources, heat pipes have found widespread use in the aerospace, and other electronics cooling industries. Modeling heat pipes before testing allows for time and labor savings by predicting system performance and limits. In this study, a model has been developed for fast and accurate determination of the thermal performance of sintered wick heat pipes. The model solves for liquid flow within the wick while assuming vapor to be at constant temperature and pressure. It considers the contribution of the shape of the interface resulting from the pressure difference between the vapor and liquid phases to the thermal resistance model. The model simplifies the voids on the liquid-vapor interface surfaces as sections of spheres with certain ratios which it can also be used as a design tool. The effect of pore radius on heat pipe performance and limits have been investigated.

Keywords: Heat pipe modeling, sintered wick heat pipes, flow through porous medium, two-phase flows

ÖZ

YÜZEY GÖZENEKLERİNDEKİ FAZ DEĞİŞİMİNİN MODELLENMESİ İLE SİNTERLENMİŞ FİTİLLİ ISI BORUSU PERFORMANSININ DEĞERLENDİRİLMESİ

Yener, Şükrü Kaan
Yüksek Lisans, Makina Mühendisliği Bölümü
Tez Yöneticisi: Prof. Dr. Zafer Dursunkaya
Ortak Tez Yöneticisi: Doç. Dr. Barbaros Çetin

Nisan 2024 , 63 sayfa

Teknolojinin gelişmesiyle birlikte, ısıl sistemlerin yönetimi giderek daha zor hale gelmektedir. Güvenilirlikleri, bakım gerektirmemeleri ve dış enerji kaynaklarından bağımsızlıkları nedeniyle ısı boruları, havacılık, uzay ve elektronik soğutma endüstrilerinde geniş bir kullanım alanı bulmuştur. Isı borularının test edilmeden önce modellemesi, sistem performansını ve limitlerini tahmin ederek zaman ve emek tasarrufu sağlar. Bu çalışmada, sinterlenmiş fitilli ısı borularının ısıl performansını hızlı ve doğru bir şekilde belirlemek için bir model geliştirilmiştir. Model, fitil içindeki sıvı akışını çözerken, buhar fazının sabit sıcaklık ve basınçta olduğunu varsayar. Model buhar ve sıvı fazları arasındaki basınç farkından kaynaklanan ara yüzey şeklini dikkate alarak ısı direnci modeline katkıda bulunur. Model, sıvı-buhar ara yüzeylerindeki boşlukları belirli oranlarda kesilmiş küreler olarak basitleştirir. Ayrıca bir tasarım aracı olarak da kullanılabilir. Gözenek yarıçapının ısı borusu performansı ve limitleri üzerindeki etkisi de çalışma içerisinde incelenmiştir.

Anahtar Kelimeler: Isı borusu modelleme, sinterlenmiş fitilli ısı boruları, gözenekli akış, iki fazlı akışlar

To my family

ACKNOWLEDGMENTS

I am deeply grateful for the unwavering support and guidance of my supervisor, Prof. Dr. Zafer Dursunkaya. Throughout my journey, he has always treated me as a valued teammate, igniting motivation and sharing invaluable wisdom in every meeting. I would like to express my sincere appreciation for his mentorship, which transcends the boundaries of academia.I would also like to express my gratitude to my co-advisor, Assoc. Prof. Dr. Barbaros Çetin, for his constructive feedback and insightful guidance, which have significantly contributed to my growth and development. I would also like to acknowledge Beste Derebaşı for her endless help and support.

I am deeply grateful to my family, Tülay, Ali, and Azra İpek Yener, for their unwavering love, support, and belief in me. Their sacrifices and encouragement have been instrumental in my journey. I am forever thankful for their presence in my life.

Special thanks to my better half, Sena Hepşen Yener, for always keeping me motivated and being my life companion on every journey. Her love and support have been a constant source of inspiration for me. I am grateful for every moment I spent with you.

Lastly, I would like to thank my team leader and manager at Turkish Aerospace Industry for their support during my M.Sc. education.

TABLE OF CONTENTS

ABSTRACT v

ÖZ vii

ACKNOWLEDGMENTS x

TABLE OF CONTENTS xi

LIST OF TABLES xiii

LIST OF FIGURES xiv

LIST OF ABBREVIATIONS xvii

LIST OF SYMBOLS xviii

CHAPTERS

1 INTRODUCTION 1

1.1 Heat Pipe Types 4

1.1.1 Cylindrical Heat Pipes 4

1.1.2 Flat Heat Pipe 5

1.1.3 Loop Heat Pipe 5

1.1.4 Variable Conductance Heat Pipe 6

1.1.5 Pulsating Heat Pipe 7

1.2 Limitations and Definitions 8

1.2.1 Surface Tension 8
1.2.2 Dry-Out 9
1.3 Literature Review 11
1.4 Motivation and Outline of Study 16
2 NUMERICAL MODEL 19
2.1 Flow Model 21
2.1.1 Interface Geometry 24
2.1.2 Thermal Model 28
3 RESULTS 35
3.1 Numerical Model Comparison 35
3.1.1 Flow Model 35
3.1.2 Thermal Model 38
3.2 Effect of Pore Radius on Thermal Performance 42
3.3 Effect of Pore Radius on Temperature Difference 49
3.4 Hypothetical Porous Media with Structured Cavities 52
4 CONCLUSION AND FUTURE WORK 55
REFERENCES 59

LIST OF TABLES

TABLES

Table 3.1 Flow Model Validation Study Parameters in [1] 36

Table 3.2 Flow Model Comparison of [1] and Current Study 38

Table 3.3 Thermal Model Validation Study Parameters in [2] 40

Table 3.4 Comparison parameters in [3] 53

LIST OF FIGURES

FIGURES

Figure 1.1 Heat pipe working mechanism 2

Figure 1.2 Wick types a) screen mesh b) grooved c) sintered [4] 3

Figure 1.3 Flat heat pipe [5] 5

Figure 1.4 Loop heat pipe [6] 6

Figure 1.5 Variable conductance heat pipes [7] 7

Figure 1.6 Pulsating heat pipes [8] 8

Figure 1.7 Heat pipe operational limits [9] 11

Figure 2.1 Solution process of model 20

Figure 2.2 Schematic diagram of flow solution domain 21

Figure 2.3 Idealization of spherical sections with specific cut percentages . 25

Figure 2.4 Modelling alternatives of spherical sections (a) Single spherical section (b) Three spherical sections (c) Multiple spherical sections . . . 26

Figure 2.5 Thermal resistance circuit 28

Figure 2.6 Schematic representation of the resistance network 29

Figure 2.7 Schematic representation and idealization pores 31

Figure 2.8 Thermal resistance network of wick interface resistance for one spherical section type 33

Figure 2.9 Thermal resistance network of wick interface resistance for all spherical sections 34

Figure 2.10 Overall thermal resistance network of a slice 34

Figure 3.1 Axial variation of liquid pressure 37

Figure 3.2 Wall temperature distribution validation with [10] and [1] 39

Figure 3.3 Schematic diagram of flat heat pipe of reference study 40

Figure 3.4 Wall temperature distribution comparison at $10\ \mathrm{W/cm^2}$ 41

Figure 3.5 Wall temperature difference comparison at $10\ \mathrm{W/cm^2}$ 41

Figure 3.6 Pore radius effect on maximum heat load 43

Figure 3.7 Non-functional spherical section types along heat pipe for various heat loads for 1.0 μm pore size 45

Figure 3.8 Non-functional spherical section types at the end of evaporator and temperature difference between two ends for various heat loads for 1.0 μm pore size 45

Figure 3.9 Non-functional spherical section types along heat pipe for various heat loads for 10 μm pore size 46

Figure 3.10 Non-functional spherical section types at the end of evaporator and temperature difference between two ends for various heat loads for 10 μm pore size 46

Figure 3.11 Non-functional spherical section types along heat pipe for various heat loads for 60 μm pore size 47

Figure 3.12 Non-functional spherical section types at the end of evaporator and temperature difference between two ends for various heat loads for 60 μm pore size 47

Figure 3.13 Non-functional spherical section types along heat pipe for various heat loads for 250 μm pore size 48

Figure 3.14 Non-functional spherical section types at the end of evaporator and temperature difference between two ends for various heat loads for 250 μm pore size 48

Figure 3.15 Effect of pore radius on temperature difference for $0.16\,\mathrm{W/cm^2}$. 49

Figure 3.16 Effect of pore radius on temperature differences for $1.6\,\mathrm{W/cm^2}$. 50

Figure 3.17 Effect of pore radius on temperature difference for $5.0\,\mathrm{W/cm^2}$. 50

Figure 3.18 Effect of pore radius on temperature difference for $16.6\,\mathrm{W/cm^2}$. 51

Figure 3.19 Available pressure head in sintered and grooved heat pipes . . . 52

Figure 3.20 Pressure distribution comparison 54

Figure 3.21 Wall temperature comparison 54

LIST OF ABBREVIATIONS

2D	2 Dimensional
3D	3 Dimensional
HP	Heat pipe
FGHP	Flat Grooved Heat Pipe

LIST OF SYMBOLS

A	Area, mm^2
d	Diameter, mm
F	Number of spherical section type
h	Height, mm
h_{fg}	Latent heat of evaporation, $\mathrm{J/kg}$
K	Permeability, m^2
L	Length, mm
M	Molecular weight, $\mathrm{kg/mol}$
P	Pressure, Pa
Q	Heat load, W
R	Thermal Resistance, $\mathrm{K/W}$
T	Temperature, K
w	Width, mm
x	x-direction
y	y-direction
z	z-direction
	Greek Symbols
$\mathcal{R}$	Radius of curvature, m
θ	Contact angle, $^\circ$
μ	Dynamic viscosity, $\mathrm{Pa \cdot s}$
ρ	Density, $\mathrm{kg/m}^3$
σ	Surface tension, $\mathrm{N/m}$
	Subscripts

ave	average
beg	beginning
con	condenser
eff	effective
evap	evaporator
f	spherical section index
int	interface
l	liquid
pc	phase change
p	pore
v	vapor
w	wick

CHAPTER 1

INTRODUCTION

Technological advances lead to rapid progress in the fields of electronics and the semi-conductor industry. Alongside the advances in manufacturing techniques, transistor sizes are gradually decreasing. With decreasing size, the number and density of transistors in integrated circuits increase exponentially in accordance with Moore's Law, which predicts a doubling of components in every 18 months [11]. Samsung Electronics, which is one of the leading manufacturers in chip industry, was producing $10\ \mathrm{nm}$ transistors in 2016. In 2023, it is using $3\ \mathrm{nm}$ transistors, and it plans to start mass production of $2\ \mathrm{nm}$ transistors in 2024 [12, 13]. Although these enhancements result in more powerful electronic devices such as computers and mobile phones, the heat fluxes are also increasing due to smaller heat dissipation area. As an illustration, in 2006, heat dissipation and heat fluxes from microprocessors were approximately $90\ \mathrm{W/cm^2}$ and $220\ \mathrm{W/cm^2}$, respectively, whereas in 2020, they have increased to $200\ \mathrm{W/cm^2}$ and $370\ \mathrm{W}$. Moreover, as reported by U.S Department of Defense, failure of electronic components increases exponentially after $75^{\circ}\mathrm{C}$ [14, 15]. In addition to failure temperature, some components require certain range of operation temperatures to ensure maximum efficiency and lifetime. Hence, thermal management is crucial to guarantee safely operating and enduring systems.

Decrease in size also comes with another challenge, reduction in heat removal area. Consequently, removing heat from a smaller area requires higher heat transfer coefficients. On the other hand, heat sinks and fins with different shapes and sizes are used to increase heat transfer area as a passive cooling technique. In air cooling systems, heat transfer coefficient could vary between 1.0 and $100\ \mathrm{W/m^2}$ depending on natural or forced convection, whereas these ranges could go up to 50 and $2500\ \mathrm{W/m^2}$ when

water cooling is implemented. Furthermore, in case of phase change is employed the effective heat transfer coefficient could rise up to $200{,}000\ \mathrm{W/m^2}$ [16]. Due to high effective heat transfer coefficient of two-phase systems, heat pipes appear to be a alternative for cooling of electronic chips.

Heat pipes are passive devices that utilize phase change phenomena to transfer heat from a heat source to a heat sink region. A typical heat pipe contains working fluid and a wick structure inside a sealed tube. Since it is a passive device, heat transfer process does not require external power. Moreover, heat pipes are stationary devices that have no moving parts. Hence, they don't require frequent maintenance and highly reliable within its operation limits.

There are three main sections inside a heat pipe which are evaporator, condenser and adiabatic sections. Heat load is applied from heat source region and it is absorbed by the working fluid. As a result, working fluid evaporates and vapor is formed. Then, the vapor travels towards condenser region where heat is rejected and liquid is formed as a result of condensation. Condensate liquid goes back to the evaporator section through the wick structure due to pressure difference. As long as there is a temperature difference between sections, heat pipe continues to operate. Fig. 1.1 is given to visualize sections of heat pipe and working cycle.

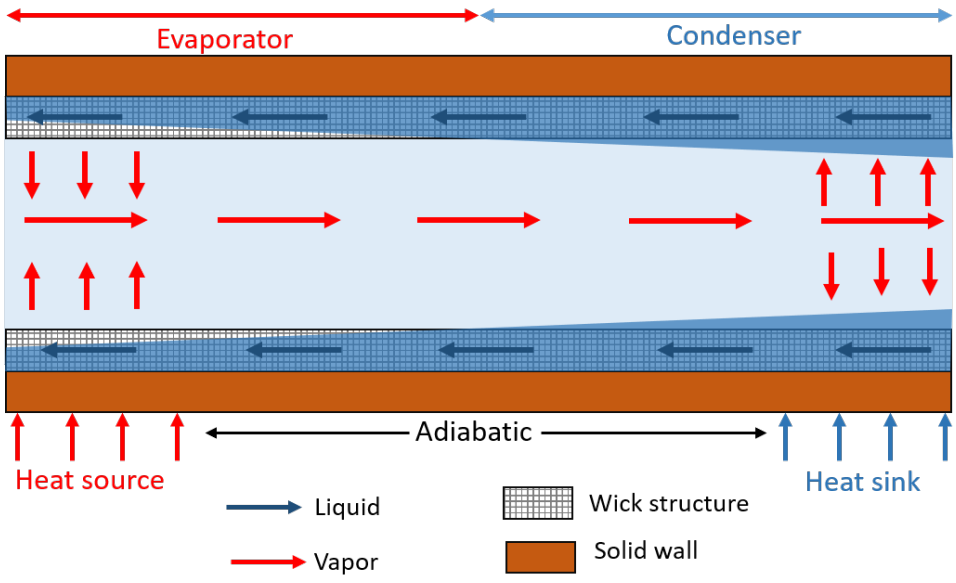

Figure 1.1: Heat pipe working mechanism

Wick structure, which creates driving force of pressure difference, plays a vital role in heat pipe characteristics and limitations. Capillary pressure must compensate pressure drop of the cycle to ensure that heat pipe works as designed. Therefore, it is important to investigate different wick types with their pros and cons. Although there exits lots of different types, three wick structures are widely used in practical applications. These are sintered, grooved and screen mesh. Following section introduces advantages, disadvantages, application areas and manufacturing aspects of wick types.

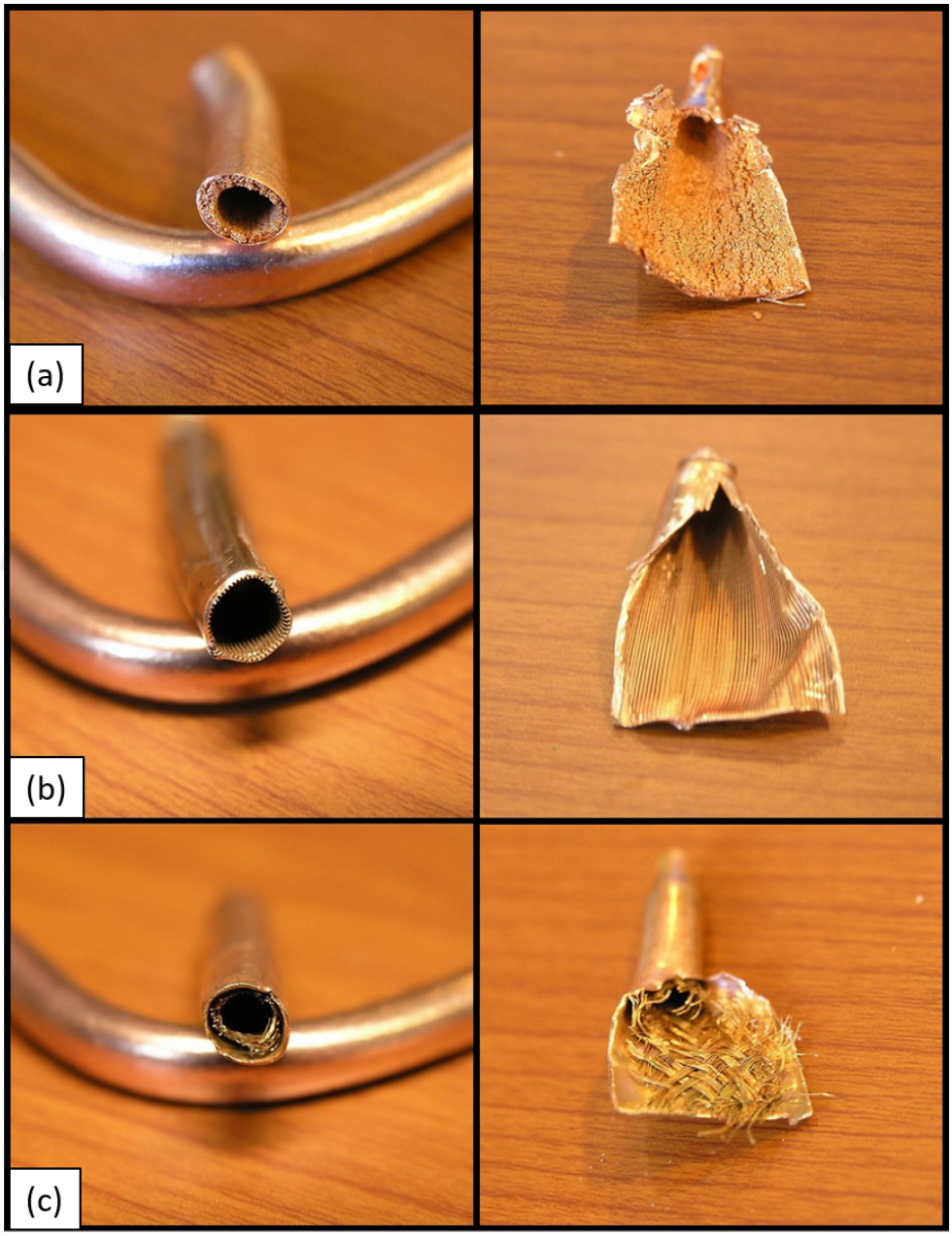

Figure 1.2: Wick types a) screen mesh b) grooved c) sintered [4]

- Screen Mesh

  Screen mesh or wire mesh wick consists of woven metal strips. Layers, size and materials of mesh structure could differ. An example of screen mesh wick is shown in Fig. 1.2. It is widely used in heat pipes since it has moderate capillary pumping without significant pressure drop. Moreover, permeability of screen mesh wick is relatively higher than sintered wick. It should be noted that diameter of wires and number of layers could affect these properties considerably.

- Grooved Wick Grooved wick type consists of channels which is attached to heat pipe wall as shown in Fig. 1.2. These channels extend from one end to another constant or variable cross-sectional area. Shape of cross-section could also differ such as rectangular, trapezoidal, triangular and circular. Although capillary pumping power is relatively lower than sintered and screen mesh wick, permeability of grooved wick is higher than others. Moreover, relatively simple channel structures allow to numerical modelling more precisely. In addition to these features, grooved wicks are easier to manufacture. Hence, it is broadly used in practical applications.

- Sintered Wick Sintered wick or powder wick is obtained by pouring powder metal onto the heat pipe wall. As seen from Fig. 1.2, it is a kind of porous medium that packed nearly spherical metal particles. Due to the structure of porous medium, permeability is lower than other wick types. On the other hand, capillary pumping power is relatively high. By this way, sintered wick heat pipes are used to discharge higher amount of heat load. Porosity and powder size distribution have a vital impact on heat pipe performance.

1.1 Heat Pipe Types

1.1.1 Cylindrical Heat Pipes

It is traditional and most common heat pipe type in industry for heat management solutions. Fundamentally, it is a sealed hollow cylindrical tube which contains wick structure and working fluid in it. It could have different type of wick structure attached

to the tube wall. Heat is applied from one end called evaporator region and rejected from the other end called condenser. Sometimes bending and flattening process is applied to heat pipe.

1.1.2 Flat Heat Pipe

Being very similar to classical cylindrical heat pipes, flat heat pipes differ from them with rectangular cross-sectional area. They mostly contain arrays of micro channels with different wick types. Furthermore, vapor channel cross-sections are available such as triangular, trapezoidal and rectangular. Depending on the application, flat heat pipes could have evaporator section at the middle of the device and more than one condenser section as illustrated in Fig.1.3. Nonetheless, their working principle is same as stated above. Occasionally, flat heat pipes are referred as vapor chambers as heat spreader.

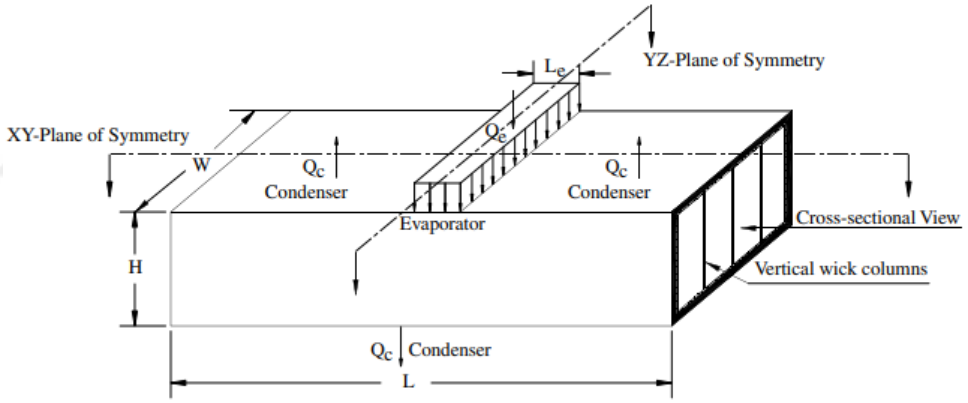

Figure 1.3: Flat heat pipe [5]

1.1.3 Loop Heat Pipe

In contrast to traditional heat pipes, loop heat pipes (LHP) have separate evaporator and condenser sections. Wick structure is placed only at evaporator section. They also have liquid reservoir called compensation chamber. Comparison to other heat pipes, LHPs could transport heat over long distances about several meters. Moreover, LHP are widely used in aerospace and electronics industry since they could operate

against gravity without significant loss of efficiency. Fig.1.4.

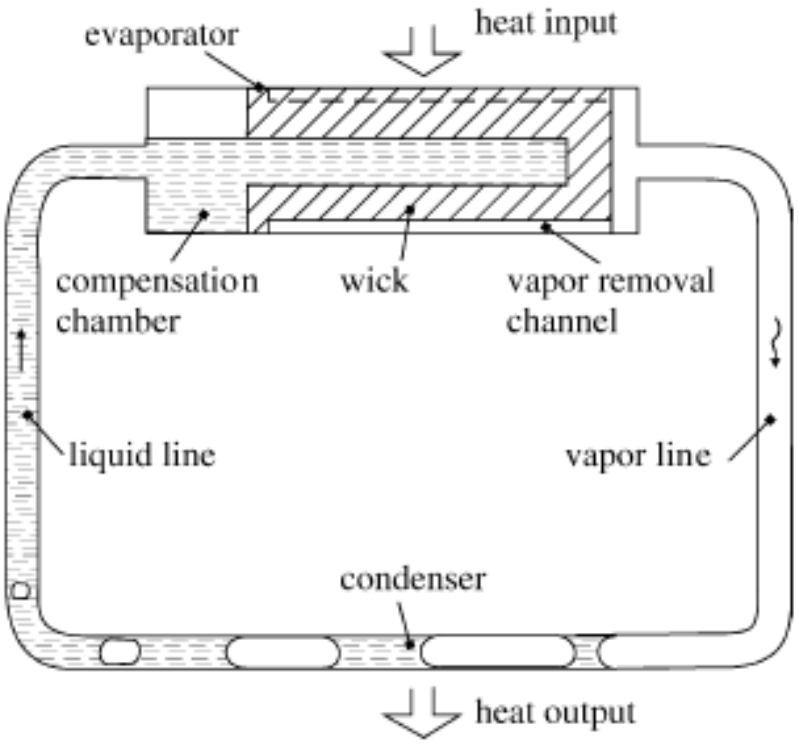

Figure 1.4: Loop heat pipe [6]

1.1.4 Variable Conductance Heat Pipe

Variable conductance heat pipes (VCHPs) are very similar to standard cylindrical heat pipes with addition of non-condensable gas. At the end of the condenser section a gas reservoir exits. Reservoir which is filled with inert gas has equal pressure to vapor pressure during steady-state operation. Whenever vapor pressure is increased due to increased saturation temperature, vapor pushes inert gas to the reservoir to ensure force balance between two fluids. As a result of pullback of inert gas, condenser length increases. Therefore, more heat is removed from evaporator and increase in temperature in heat load surface is prevented. On the contrary, whenever heat load is decreased, vapor temperature and pressure is decreased. So, inert gas expands and condenser length shortens as illustrated in Fig.1.5. By doing this, over-cooling is prevented. VCHPs are widely used in space industry.

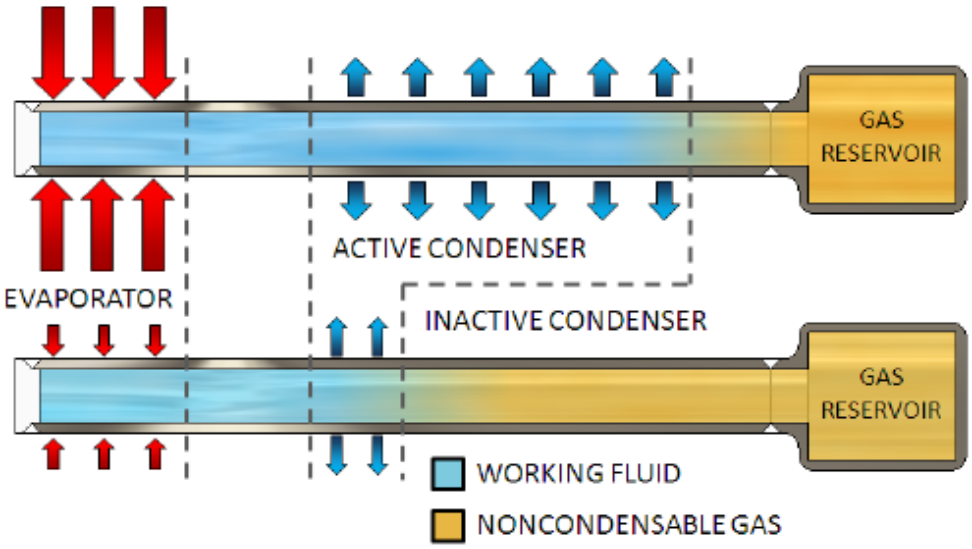

Figure 1.5: Variable conductance heat pipes [7]

1.1.5 Pulsating Heat Pipe

Pulsating heat pipes (PHPs) which is sometimes called as oscillating heat pipes (OHPs) are relatively new type of heat pipe family. They are invented by Akachi in 1993. Unlike other heat pipes, pulsating heat pipes (PHPs) have no wick structure in it. It consists of a bent tube which alternating direction in between evaporator and condenser sections with several turns as illustrated in Fig.1.6. Tube is vacuumed and filled with working fluid. It has two main configurations based on whether it is closed (CLPHP) or open loop (OLPHP). In both configurations, working fluid absorbs the heat from evaporator and forms local bubbles. Vapor and liquid slug due to pressure difference and heat is rejected in condenser section. Condensation occurs and cycle continues until temperature difference between two sections are exist.

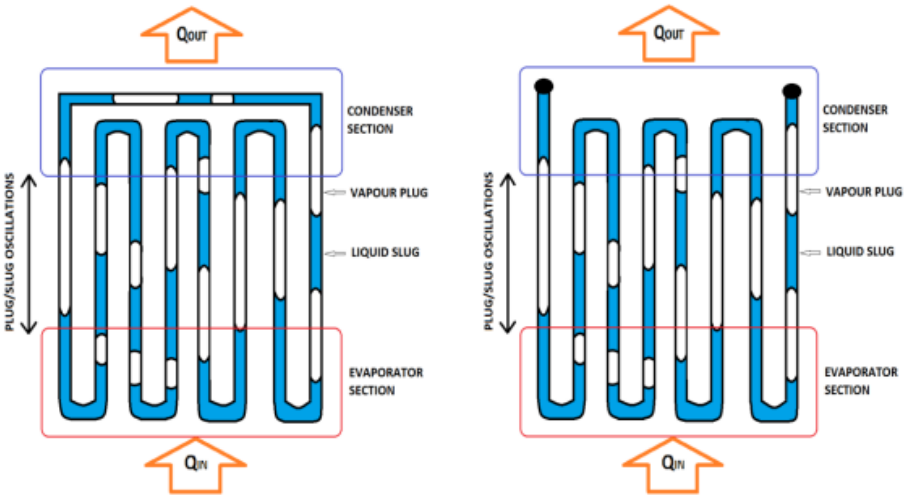

Figure 1.6: Pulsating heat pipes [8]

1.2 Limitations and Definitions

In this section operational limitations of heat pipe and some important physical definitions are discussed.

1.2.1 Surface Tension

Molecules,which sit at the free surface or interface of the liquids, have lower cohesive forces than molecules in the bulk. The missing binding energy leads increasing surface energy. Positive surface energy density against a vacuum or gas ensures tendency to the minimum interface area. The surface energy density is called as surface tension and defined as normal force per unit length [17].

As a direct consequence of surface tension on a curved surface is pressure difference across interface. This pressure difference mostly named as capillary pressure. It is related to surface energy density and radius of curvature of the surface. Relation is defined by Young-Laplace equation given in Eq.1.1.

$$\Delta P = P_c = P_v - P_l = \sigma \left(\frac{1}{R_1} + \frac{1}{R_2} \right) \tag{1.1}$$

Where, R_1, R_2 corresponds to two principal radii of curvature, P_v is vapor pressure, P_l is liquid pressure and σ is the surface tension. For a spherical surface two principal directions are same. So Eq.1.1 could be written as Eq.1.2 where, R is the radius of the sphere.

$$\Delta P = P_c = P_v - P_l = \frac{2\sigma}{R} \tag{1.2}$$

1.2.2 Dry-Out

Dry-out is a phenomenon that insufficient amount of liquid exist at the evaporator section and heat pipe loses its functionality. It could be initiated with several reasons. These reasons lead to heat pipe limits including capillary limit, boiling limit, sonic limit, entrainment limit and viscous limit.

- **Capillary Limit**: As discussed in 1.2.1, pressure difference exist between two phases and it is called as capillary pressure. At the evaporator section of a heat pipe, radii of curvature is lower than the condenser section. Hence, liquid pressure at the condenser is higher than the evaporator according to Eq. 1.1. This pressure difference is the main driving force which pulls liquid back to evaporator. Heat pipe will not continue its normal operation whenever the capillary pressure is inadequate to compensate total pressure loss of the heat pipe [18].

  $$\Delta P_{c,max} \geq \Delta P_l + \Delta P_v + \Delta P_g \tag{1.3}$$

  In Eq.1.3 ΔP_l and ΔP_v corresponds to pressure drop of liquid and vapor respectively. Moreover, ΔP_g is the pressure drop due to gravitational effects if heat pipe is inclined. Gravity effect could be positive or negative depending of angle of inclination.

- **Boiling Limit**: At high heat fluxes, nucleate boiling could occur at evaporator. Bubble formation inside the wick structure results in vapor blanket. Ultimately,

capillary action is blocked and wick will dry out with excessive heat load. This phenomenon also called as burnout [18].

- **Sonic Limit:** It is chocking condition of heat pipe which mostly occurs in start-up phases for low vapor density liquids such as liquid metals. In chocked condition, a higher temperature gradient exist in axial direction and nearly isothermal characteristic of heat pipe is lost. Sonic limit doesn't necessarily results with dry out [19].

- **Entrainment Limit:** In a heat pipe, liquid flows from condenser to evaporator where vapor flows in opposite direction. Both phases experience a shear force at the interface. If the magnitude of shear force high enough to prevent liquid flow, then dry out occurs. Weber number given in Eq.1.4 is a conventional dimensionless parameter which describes ratio of vapour forces to liquid surface tension [20].

$$We = \frac{\rho_v v^2 z}{\sigma} \tag{1.4}$$

  where ρ_v, v and z are vapor density, vapor velocity and characteristic length which is vapor spacing for a heat pipe respectively. Typical limit for entrainment is could be assumed as We number equals to 1. On the other hand, Kim *et al.* reported that critical Weber number is in range of $0.2 - 20$ [21].

- **Viscous Limit:** At low operating temperatures vapor pressure at the evaporator could be very small and nearly same order of magnitude with the required pressure gradient to ensure vapor flow to the condenser. Hence, vapor pressure may not be sufficient to increase flow through condenser and it is called as viscous or vapor pressure limit.

Typical heat pipe performance limits are given with respect to operational temperature at Fig.1.7. Red zone indicates where heat pipe works as it designed. The performance map is unique for each heat pipe and could alter based on type and dimensions of heat pipe.

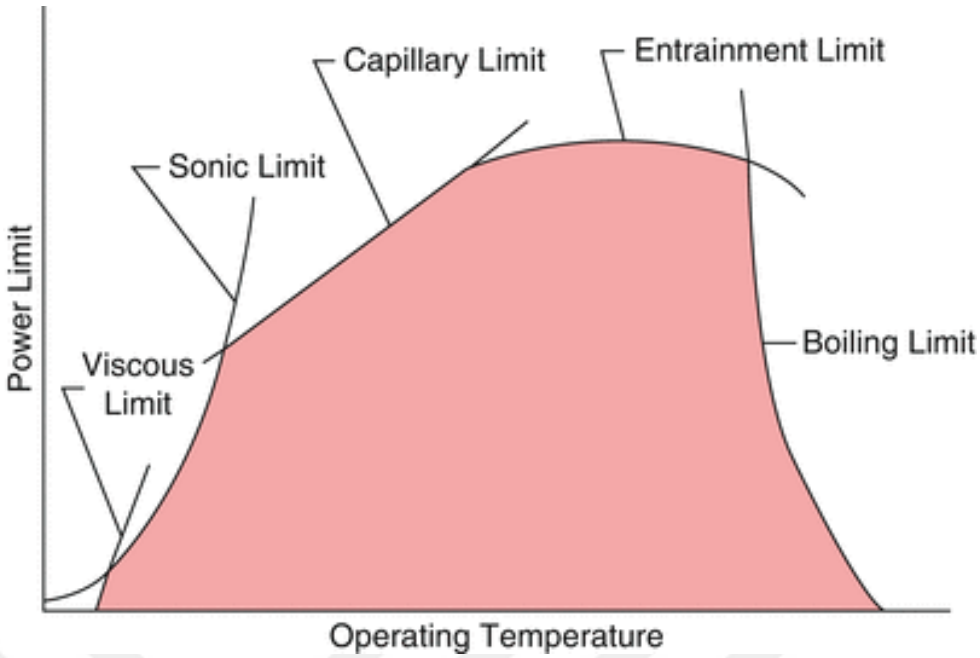

Figure 1.7: Heat pipe operational limits [9]

1.3 Literature Review

In 1856, the French engineer Henry Darcy introduced his flow trough porous medium equation, which is still in use with his name today [22]. In his experiments with silica sand from Saône river, he measured the pressure drop across sand volume at various flow rates at constant temperature. So, he proposed Eq.1.5 to correlate pressure drop and velocity at constant temperature where he called k as hydraulic conductivity.

$$\frac{\Delta P}{L} = \frac{U}{k} \tag{1.5}$$

Despite being the pioneering work in its field, there is a deficiency in the original Darcy equation: the viscosity effect. Hazen [23] introduced viscosity effect indirectly by adding temperature correction terms to equation. The establishment of viscosity on its own was achieved through repeated experiments with different liquids. The explicit inclusion of viscosity in the equation resulted in the formulation of the Darcy equation as known today [24, 25].

For turbulence flow through porous medium, Forchheimer suggests to add a term which contains velocity square to original Darcy equation. He called extra term as a form term caused by drag force [26].

Two nodes thermal resistance network model is developed by Ababneh *et al.* [27]. Study considers a planar heat pipe which contains non-condensable gases at the condenser section. Sintered porous wick is considered with average pore diameter of 11.7 μm. Resistance model considers axial conduction in wick and wall whereas it neglects convection in fluid. So axial energy transport is purely by diffusion. Resistance at the liquid-vapor interface is provided through experiments as a function of temperature difference. Wick conductivity is calculated by Maxwell's equation. Liquid pressure drop is given by Hagen-Poiseuille equation which is applicable to laminar, viscous and incompressible flow in channel. Permeability is calculated from Chi equation as a function of porosity.

Vadakkan *et al.* [28] developed a three dimensional model to analyze both steady and transient performance of sintered copper wick flat-plate heat pipes with multiple discrete heat sources. Momentum and energy equations in bot vapor and liquid phases are solved. Forchheimer model for liquid flow inside the wick is employed. Moreover, interface mass flux is calculated through kinetic theory and Clasius-Clapeyron equation. Wick parameters such as permeability and conductivity is taken from a commercial heat sink.

A similar three-dimensional model is used by Ranjan *et al.* [2]. In addition to [28] model, contact angle and interface surface shape is accounted through wick level micro model. Meniscus area between two copper wire is calculated. Flat to curved area ratio is applied to macro model as area correction term as a function of porosity and contact angle. As a result, 16% higher temperature drop is obtained relative to macro model which is not consider interface shape.

Zehgari *et al.* [29] modelled a flat miniature heat pipe and conducted experiments for different tilt angles. For pressure drop of liquid in sintered porous wick, they used Hagen-Poiseuille equation as in [27]. They used two nodes thermal resistance network model. Moreover, bunch of equations for evaporation and condensation heat transfer coefficients are given from literature. Operating temperature is verified

through experiments and pressure drop is compared with Kaya and Goldak.

Multidimensional heat transfer in a rectangular grooved heat pipe is modeled by Odabaşı [30]. In the, phase change heat transfer is introduced to the study as a boundary condition, where evaporation and condensation models at the liquid-vapor interface are solved.

A grooved-sintered hybrid wick type heat pipe is modelled and conducted experiments to compare results by Li *et al.* [31] . Figure X illustrates the wick type which is used in the study. Two nodes thermal resistance network is used for heat transfer. On the other hand, liquid flow and pressure drop inside composite wick structure are not investigated. Effect of shape of the interface is considered however, interface shape and contact angle is assumed to constant. Moreover, area ratio of sintered particles to evaporative area is given with a correlation. It is stated that up to $50\ \mathrm{W}$ of heat load, model has an agreement with the experiments.

Ferrandi *et al.* [32] developed a model to simulate both steady and transient operation of sintered wick heat pipes by using thermal resistances and capacitors lumped model. Heat pipe divided into three sections as evaporator, adiabatic and condenser. In wick structure only conduction is considered in line with radial and axial resistances. In the fluidic model both vapor and liquid flow is considered. In liquid flow Darcy equation is used and form effects are neglected in contrast to [28]. At the liquid vapor interface Young-Laplace equation is used with capillary radius is equal to 41% of grain radius. They concluded their study as grain radius is not vital importance for overall resistance. However, it seriously determines the dry-out limit of heat pipe.

Nookaraju *et al.* [33] investigated sintered wick heat pipe operation both experimentally and numerically by using commercial computational fluid dynamics software Fluent. In the experiment, a heater is used at the evaporator and cooling jacket is used at the condenser section. Moreover, thermocouples are placed at two ends. They observed that deviation at the evaporator section are much more than condenser section when experiments and numerical data is compared.

Zeghari *et al.* [34]. experimentally investigated fill ratio effects at a flat heat pipe with a sintered copper wick. 10 thermocouples on the surface for wall temperature and one

internal thermocouple for vapor temperature are placed in experiment. Moreover, hysteresis phenomenon is also investigated through ascending and descending heat loads. Vapor temperature and wall temperature are recorded and thermal resistance is calculated for different fill ratios. It is concluded that 25% of fill ratio is optimum in terms of thermal performance of a heat pipe.

As in [31], Zhu *et al.* [35] investigated thermal performance of composite wick structure for a thin flat heat pipe. In their experiment, heat load is applied at a local section of evaporator region instead of whole evaporator section. To investigate effect of particle size of grains, porosity and width of the grooved channels, six different specimens are fabricated. Cooling at the condenser is provided through a cooling block with constant water temperature. They concluded that smaller grain radius could be helpful to decrease thermal resistance of a composite wick heat pipe.

Sangpab *et al.* [36] developed a mathematical model to predict wall temperature and thermal resistance of bent and flattened heat pipes with sintered wick. Both liquid and vapor flow are considered. Darcy equation is used while solving liquid flow inside the wick. Finite element method is used for the governing equations. They verified the model with Kaya and Goldak's study for sintered wick heat pipes. Their work is particularly focuses on different bent and flattened circumstances which cause sharp increase in thermal resistance and reduce thermal performance of heat pipe.

Zhang *et al.* [37] fabricate wick structures with different powder types such as irregular or spherical. Each wick type has different powder size distribution and porosity ratio. They experimentally investigated pressure drop versus flow rate, contact angle, capillary rising height and droplet wicking time. They used obtained data to calculate permeability of each wick with using Darcy equation. Results showed that spherical powders have lower permeability but higher capillary rising due to their formal shapes.

Tsai *et al.* [38] investigated both dendritic and spherical shape powders experimentally. In their study, they fabricated sintered wicks which has different porosity and powders size in both powder shape. In the experiment, powder structure is sintered on a metal bar which is heated from bottom with a constant heat flux. Water is supplied to wick structure as a working fluid to dissipate heat from metal block. Thermocou-

ples are placed on the metal block to measure temperature and evaluate wick performance. Both wick thermal conductivity, and evaporative heat transfer coefficient is calculated. It is stated that smaller and spherical powder size leads to higher thermal conductivity whereas dendritic powders have better evaporative heat transfer.

Similar to [37],Deng *et al.* [39] investigated permeability and capillary rising height for different types and sizes of powders. Permeability is calculated from Darcy equation by using experimental data. In addition to [37] they also included different type of working fluids to see compatibility with powder material and fluid. Range of powder sizes are given in between 3 μm and 110 μm. It is stated that copper powder has higher permeability than nickel but working fluid is also important.

Choi *et al.* [40] experimentally investigated permeability and effective thermal conductivity of a sintered wicks. Darcy equation is used to calculate permeability and thermal conductivity is obtained through laser flash method. They compared the both permeability and wick conductivity results with correlations to see difference. It is stated that deviation of correlations from experiments in terms of permeability increases with decreasing pore radius.

Jasper [41] conducted a comprehensive literature survey about surface tension. He compiled surface tension studies spanning from the 19th century up to 1969 and tabulated surface tension values for 2200 different liquids. Method of measurements, purity of liquids and accuracy of experiments are given if it is available at the original study. Moreover, he proposed a temperature dependency equation in the form of $\sigma = a + bT$.

Busse [42] investigated heat pipe limitations for cylindrical heat pipes. Limitations are classified in two main categories as insufficient flow from condenser to evaporator region and vapor flow related limitations. In his work, he introduced how to calculate ultimate limits of heat pipe analytically such as sonic limit and viscous limit.

1.4 Motivation and Outline of Study

The objective of the study is to develop a thermal model to evaluate thermal performance of sintered wick heat pipes by modeling phase change in surface pores rather than using effective heat transfer coefficient.

As summarized in the previous sections, heat pipes pose a great potential in terms of thermal management due to reasons such as not requiring external power, having no moving parts, carrying high heat fluxes with low temperature differences and not requiring maintenance and high reliability. Hence, heat pipes are widely used in thermal management solutions.

As seen in the literature review, heat pipes have been the subject of numerous studies due to their wide-ranging applications in various industries. Experimental studies aim to determine the limits and performance of heat pipes under different conditions by creating a specific set of test parameters. However, factors such as creating suitable conditions for the production and environment make experimental studies time-consuming and resource-intensive. Hence experimental studies for thermal management systems are time-costly and expensive.

Numerical studies, as an alternative to experimental research, provide fast results in determining the limits and performance parameters of heat pipes. However, excessive simplifications in the modeling process can lead to results that are far from reality. It is important that the numerical models are detailed enough to simulate the real-world situation, but simple enough to provide fast results.

Sintered wick heat pipes present a challenge for numerical modeling. In most studies, a permeability factor is used to model the liquid flow, while the phase change at the liquid-vapor interface is modeled with an equivalent constant heat transfer coefficient.In this case, numerical studies are dependent on experimental correlations. When these correlations are used for heat transfer, the contact angle on the interface surface and the distribution of voids are not taken into account. The limit of the heat pipe can only be determined based on pressure. One of the primary objectives of this study is to simulate sintered wick heat pipes, taking into account the effect of the interface shape and contact angle on phase change heat transfer.

In his PhD thesis, Saygan developed a tool called H-PAT (Heat Pipe Analysis Tool) for fast and accurate modeling of grooved wick heat pipes [43]. With H-PAT, it is possible not only to analyze but also to design grooved wick heat pipes. In the study, fluid flow and temperature are solved whereas, vapor pressure and temperature are assumed to be constant at saturation temperature and pressure [43]. Derebaşı expanded H-PAT to solve vapor flow and temperature in her thesis [44]. The secondary objective of this study is to expand the H-PAT for use in the design and analysis of sintered wick heat pipes. In this manner the thesis is organized as follows.

In Chapter 1, importance of thermal management and heat pipes is explained. The working principles and classification of heat pipes are stated. In addition, the advantages and disadvantages of different wick types are discussed. Physical concepts are also mentioned to create background about heat pipe limitations and performance parameters. Moreover, the literature review aims to demonstrate how this thesis differs from previous studies by showcasing past research on sintered wick heat pipes.

In Chapter 2, the methodology used in the study is explained. It describes how the fluid flow is simulated, how the thermal resistance model is established, and how the phase change at the vapor-liquid interface is modeled. Assumptions for solution domain are given with their reasons. Additionally, simplification of the shape of the liquid filling cavities at the interface and modeling of cavities with different geometries are explained in this section. In Chapter 3, the modeling approaches used for thermal and fluid flow are compared with those in other studies found in the literature. It has been observed that the model used in the current study provides consistent results with the findings of other studies. Additionally, a comparative study between grooved and sintered wick heat pipes of the similar dimensions has been conducted. The differences between these two types of heat pipes in terms of operational conditions and limits have been explained. Pore radius effect on maximum heat load and temperature difference at a constant heat load is given. Moreover, effect of non-functional cavities at the interface for different spherical sections is studied at the section. In Chapter 4,the significant points of the study have been emphasized, and some recommendations for future research have been provided.

CHAPTER 2

NUMERICAL MODEL

In this study, an analysis and design tool has been developed for the sintered wick heat pipe, as illustrated in Fig.1.2. While the liquid flow within the wick is solved in the study, the vapor flow is not considered. The vapor is assumed to be at the saturation temperature and constant along the heat pipe. The pressure drop occurring in the vapor phase is neglected compared to the liquid within the wick, as it is expected to be significantly lower. Additionally, the vapor pressure is considered constant along the heat pipe and equal to the saturation pressure.

To generate a solution, the model requires information about the geometry of the heat pipe and the wick, the type of fluid, cooling conditions, and heat load. These details include geometric parameters such as length of the heat input and heat sink regions, wall and wick thickness, as well as porosity of the wick and pore radius. Additionally, information on the coolant temperature and its convection heat transfer coefficient, and total heat load are needed. The model discretizes the heat pipe into small incremental sections based on the input parameters. Heat and flow equations are solved within each section. Furthermore, considering the conservation of mass, phase changes within each section are also calculated.

The calculation begins by initially estimating the ratio of heat transferred through phase change at a constant vapor temperature. Using conservation equations, the pressure and flow rate of the liquid within the wick are determined. After calculating the liquid pressure, the radius of curvature and contact angle for each spherical sections are computed for each incremental sections. This process results in the extraction of the surface shape. These parameters are utilized both to check for the existence of dry-out within the heat pipe and to provide inputs to the thermal model.

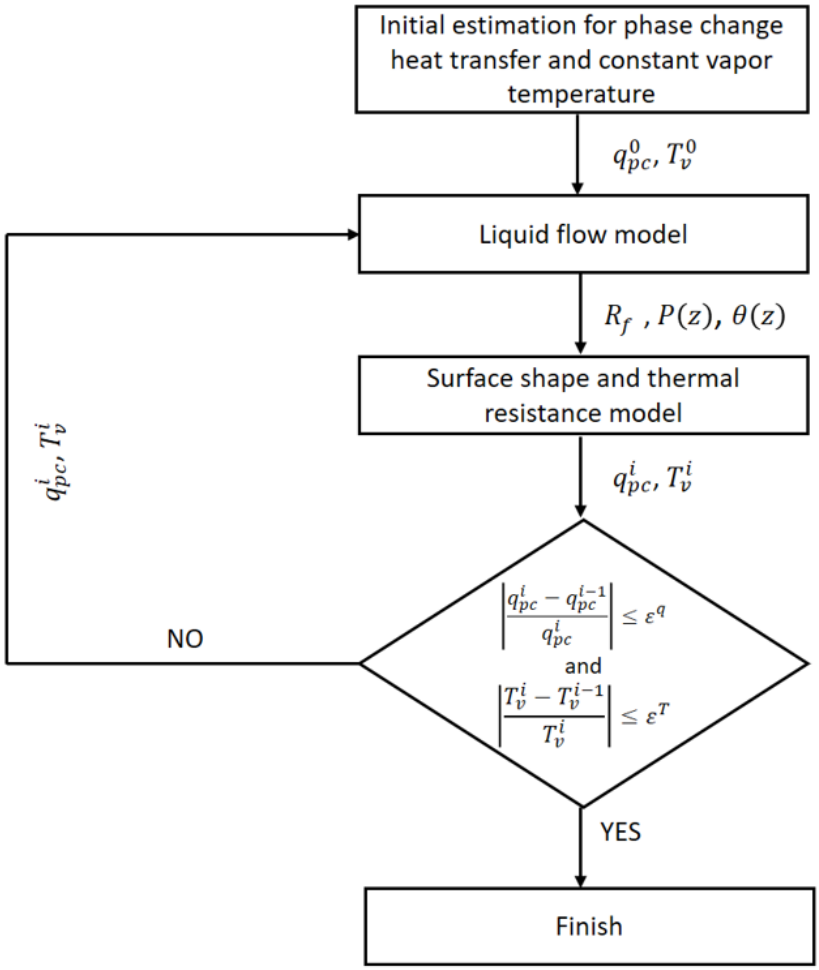

Figure 2.1: Solution process of model

The thermal model constructs a quasi 3D thermal resistance network subject to simplifying assumptions. It calculates thermal resistances for the wall, wick, and phase change as well as axial conduction. After the solution, distribution of wall temperature, vapor temperature, and heat transferred through phase change are obtained within the thermal model. By comparing the initial input values with the solution results, convergence is calculated. If the difference between two consecutive iterations exceeds specified limits, a new iteration is initiated and the procedures continues until converge. The flowchart illustrating the solution methodology is shown in Fig.2.1.

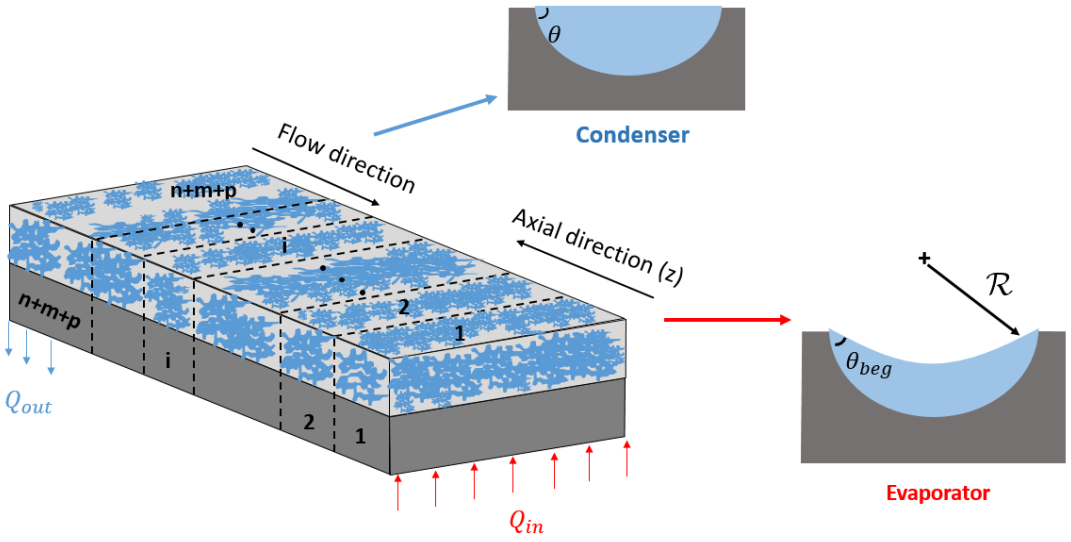

Figure 2.2: Schematic diagram of flow solution domain

2.1 Flow Model

In order to obtain pressure inside the wick region and surface shape, the flow model utilized in the study has been developed. The liquid flow inside cavities of the wick region in the order of hundreds of micrometers whereas vapor spacing of a typical heat pipe is around in the order or millimeters. Hence, liquid pressure drop is expected to be more critical due to higher pressure drop in the wick region. Therefore, vapor pressure drop as well as the viscous effects at the interface may be safely neglected [45]. Instead, the vapor pressure is assumed to be equal to the saturation pressure at the saturation temperature and remains constant along the heat pipe. The model solely resolves the liquid flow within each slice. A representative schematic is given at Fig. 2.2.

The following assumptions were made during the model development:

- Liquid flow is steady, laminar, and incompressible.
- Vapor pressure drop is relatively smaller than liquid pressure drop and it is negligible.
- The liquid flow along the heat pipe is unidirectional.
- Liquid flow is driven by the pressure gradient, with no other factors involved

(e.g., gravity).

- The incremental sections are sufficiently small for pressure changes to be negligible; therefore, the pressure within each section is constant.

The calculations for the mass flow rate within the wick are determined using the heat transferred through phase change. Eqs.2.1–2.3 indicate that the mass flow rate increases approximately linearly in the condenser, reaches its maximum value at the section between the condenser and evaporator, then decreases approximately linearly in the condenser section. Further details of flow model calculations could be found in [43].

$$\dot{m}_l(z_i) = C_{1,i} z_i + C_{0,i}, \quad L_a \leq z \leq L_c \tag{2.1}$$

$$\dot{m}_l(z_i) = A_{1,i} z_i + A_{0,i}, \quad L_e \leq z \leq L_a \tag{2.2}$$

$$\dot{m}_l(z_i) = E_{1,i} z_i + E_{0,i}, \quad 0 \leq z \leq L_e \tag{2.3}$$

Since the liquid flow inside the wick is assumed laminar, uni-directional and driven by pressure gradient. Therefore, Darcy pressure drop equation is applicable for flow through porous medium [46].

$$\frac{dp}{dz} = \frac{\mu}{\rho A K} \dot{m} \tag{2.4}$$

where K is the permeability and A is the cross-sectional area of the flow. In Eq. 2.4 permeability refers to the ability of the working fluid to pass through the wick structure. It is s a characteristic feature of the wick structure and depends on geometrical parameters such as porosity (ϵ) and pore diameter (r_p). There are many correlations available to calculate the permeability of the wick structure based on experimental data. In the current study, permeability is calculated as given in Eq. 2.5 [47].

$$K = \frac{(2r_p)^2 \epsilon^3}{360(1-\epsilon)^2} \tag{2.5}$$

A factor κ could be defined to establish a linear relationship between pressure drop and liquid flow rate. By combining the terms other than the mass flow rate in Eq. 2.4, pressure drop equation could written as

$$\frac{dp}{dz} = \kappa \cdot \dot{m} \tag{2.6}$$

where,

$$\kappa = \frac{\mu}{\rho A K} \tag{2.7}$$

By combining Eqs. (2.1–2.3) and Eq. 2.6, liquid pressure distribution inside the wick can be found. The resulting pressure distribution equations for each section of the heat pipe are expressed in the following manner:

$$p(z) = \int (E_1 z + E_0) \cdot \kappa \, dz, \quad 0 \leq z \leq L_e \tag{2.8}$$

$$p(z) = \int (A_1 z + A_0) \cdot \kappa \, dz, \quad L_e \leq z \leq L_a \tag{2.9}$$

$$p(z) = \int (C_1 z + C_0) \cdot \kappa \, dz, \quad L_a \leq z \leq L_c \tag{2.10}$$

In order to solve Eqs. (2.8–2.10), two boundary conditions need to be specified. First boundary condition comes from dry-out condition of a heat pipe. At the beginning of the evaporator, edge angle cannot be lower than the material contact angle unless dry-out occurs. So, by using Eq. 1.2, pressure at the beginning of evaporator could be calculated. First boundary condition is determined as follows :

$$p\Big|_{z=0} = p_v - \frac{2\sigma \cos(\theta_{ca})}{R_{z=0}} \tag{2.11}$$

Moreover, pressure gradient at the end of the condenser and mass flow rate of liquid is zero. So, second boundary condition could be obtained from zero pressure gradient condition.

$$\frac{dp}{dz}\bigg|_{z=L} = 0 \tag{2.12}$$

After pressure and mass flow rates are obtained, surface shape is created by using radius of curvature and contact angle at each section by using the Young-Laplace equation. Since amorphous cavities are modelled combination of many spherical sections, contact angle for each spherical section type is different at same pressure difference. Spherical sections with higher cut ratio have higher contact angle whereas spherical sections with lower cut cut ratio have lower contact angle. Moreover, contact angle can not be lower than the material contact angle. Hence , it means that spherical

sections with lower cut ratio could be non-functional at the same radius of curvature while spherical sections with higher cut ratio is functional. Details about the spherical sections are given in the following section. Lastly, surface shape of spherical sections are transferred to the thermal module of the model to form the thermal resistance network and to obtain converged solution.

2.1.1 Interface Geometry

As previously mentioned, porous media contain amorphous cavities. These amorphous cavities exist both at the core of the medium and the vapor interface. To calculate liquid pressure drop within the wick experimental correlations are used. These experimental correlations are also available for effective heat transfer coefficient. However, these effective heat transfer coefficient correlations are insensitive to the contact angle and surface shape at vapor interface. So, one single coefficient is used through heat pipe when experimental heat transfer coefficients are employed. However, when modeling heat transfer at the interface, the shape of these amorphous cavities and contact angle become significant since phase change heat transfer occurs predominantly in thin film region. The size and shape of these cavities determine the contact angle and the heat transfer area, making them crucial for heat transfer considerations. Due to the importance of these cavities on the interface surface for heat transfer, in this study these cavities are simplified and modeled. By doing so, heat transfer model of current study becomes contact angle sensitive and an effective heat transfer coefficient is obtained that varies along the heat pipe. A separate section has been included in the study to explain how to model them.

Interface cavities where liquid and vapor phases meet are idealized as spherical sections. At the interface between the porous medium and the vapor phase, many different geometries of spherical sections could exist, as many different types of amorphous cavities exist. Simplification of these cavities to spherical sections is illustrated in Fig. 2.2. It is assumed that these spherical interface cavities have connections with the core of the porous medium. Additionally, these amorphous cavities are modeled as sections of a sphere cut with a certain percentage as shown in Fig. 2.3. A complete sphere is represented by 100% cut ratio, whereas a 50% cut ratio represents a

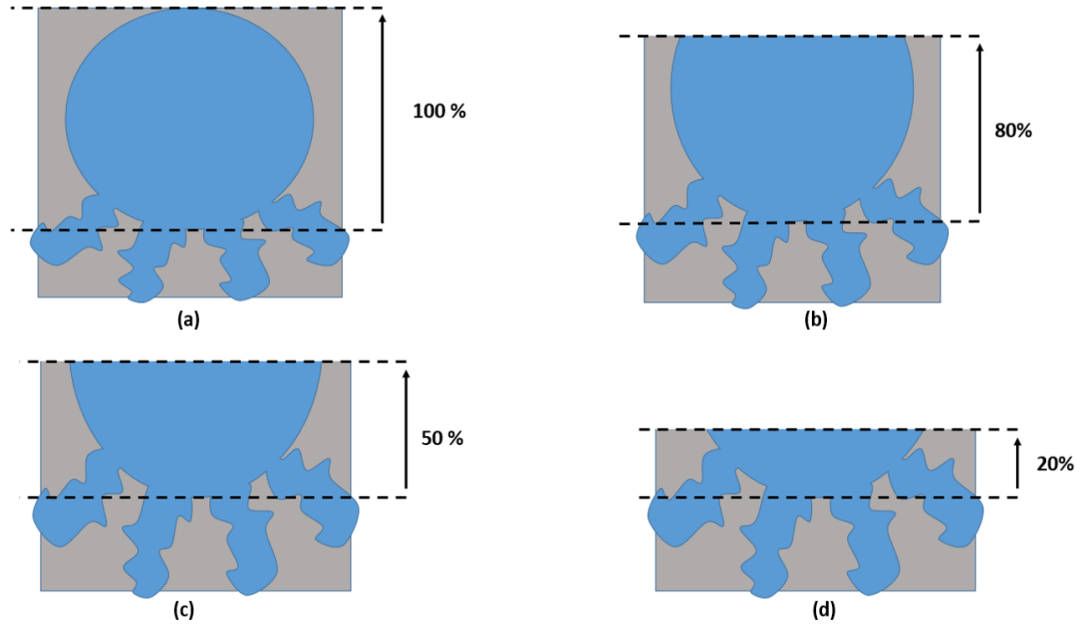

Figure 2.3: Idealization of spherical sections with specific cut percentages

hemisphere.

Idealization from amorphous cavities to spherical sections with specific cut percentages are given in Fig. 2.3. When modeling amorphous cavities, one or more spherical sections can be used in combinations. In H-PAT, user could specify how many number of different spherical sections are used for both design and analysis cases. In Fig. 2.4, different modelling alternatives are illustrated. In case (a) a single spherical section is used through heat pipe which is a hemisphere. In case (b) three different spherical sections are used with equal spacing in terms of cut percentages. Moreover, modelling idea could generalized as shown in case (c) with a finite number of different spherical sections. While modelling interface amorphous cavities with combinations of multiple spherical sections, cut percentage of middle spherical section is set to 50% and others are spherical section percentages distributed with equal spacing of cut ratios.

As stated, users could define the number of different spherical sections to model the interface. Increasing the number of spherical section types results in a more realistic modelling. However, computational cost also increases as number of spherical section types increases.

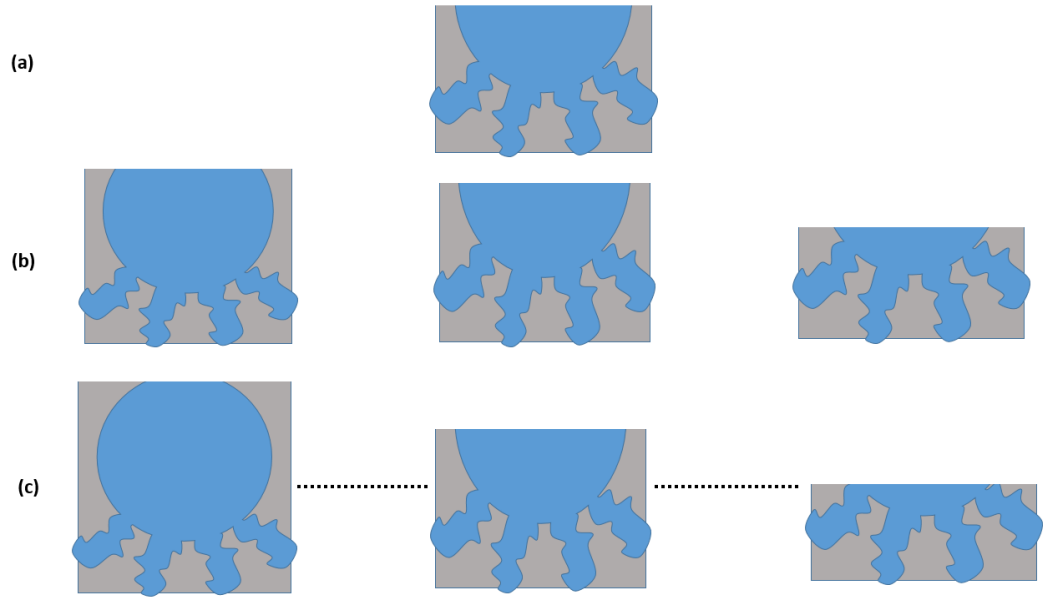

Figure 2.4: Modelling alternatives of spherical sections (a) Single spherical section (b) Three spherical sections (c) Multiple spherical sections

It is assumed that at each slice of the solution domain is identical in terms of pore size and number of spherical sections. Each discrete section of solution domain has the same number of different spherical section types. To obtain a solution, the user provides input on one single pore radius and the number of different spherical sections on the interface surface. Cut ratios of these spherical sections could be provided by the user or automatically determined from H-PAT as equal spacing. For example, a user can specify that there will be 3 different cut ratios on the interface surface, with these ratios being 30%, 50%, and 80% to simulate the phase change. Each slice contains spherical sections with the three specified cut ratios.

To calculate thermal resistance in each slice, it is essential to determine the number of spherical sections for each spherical section type. The distribution of these different types of spherical sections in the solution domain is based on the assumption that the total area occupied by each spherical section is equal.

Total interface heat transfer area at each slice could be calculated by using porosity factor. Eq. 2.13 is given for a slice at the evaporator section but it is applicable for other sections as well.

$$A_{int,T} = w_{hp}\frac{L_e}{n}\epsilon \tag{2.13}$$

where ϵ is the porosity, L_e/n is the length of the slice and w_{hp} is the width of the heat pipe. $A_{int,T}$ is the total interface phase change area for one section. The remaining part of the total slice area is assumed to be the solid wick material and is impermeable to liquid-vapor interaction. Moreover, it is assumed that each spherical section with a different cut ratio occupies the same amount of area. Total area occupied by one spherical section could be calculated as:

$$A_{int,f} = \frac{A_{int,T}}{F} \tag{2.14}$$

where F is the number of spherical section type which is provided by the user. So, $A_{int,f}$ is the total area occupied by spherical sections which has the same cut percentage. Subscript f is the spherical section index which stands for one specific spherical section. Here it would be more useful to illustrate the situation with an example.

One could specify that there will be three different spherical sections with cut percentages of 25%, 50% and 75%. In such a case, F is equal to 3. Moreover, for spherical sections with the cut ratio of 25%, f is 1 since 25% is the smallest cut ratio. For 50% and 75%, f is 2 and 3 respectively. For phase change heat transfer area which is occupied by each spherical section types could be calculated as:

$$A_{int,1} = A_{int,2} = A_{int,3} = \frac{A_{int,T}}{3} \tag{2.15}$$

In a slice of computational domain, there are many spherical sections which have same the cut percentage. So, the number of spherical sections that belongs to the same cut percentage can be determined by using projected tip area as given in Eq.2.16.

$$N_f = \frac{A_{int,f}}{A_{prj,f}} \tag{2.16}$$

2.1.2 Thermal Model

A quasi 3D resistance network model is generated to calculate wall and vapor temperatures. Model accounts for both axial and transverse conduction resistances through heat pipe wall and wick structure. Moreover, phase change heat transfer is implemented as a thermal resistance to the circuit. Fig. 2.5 illustrates the overall thermal resistance circuit.

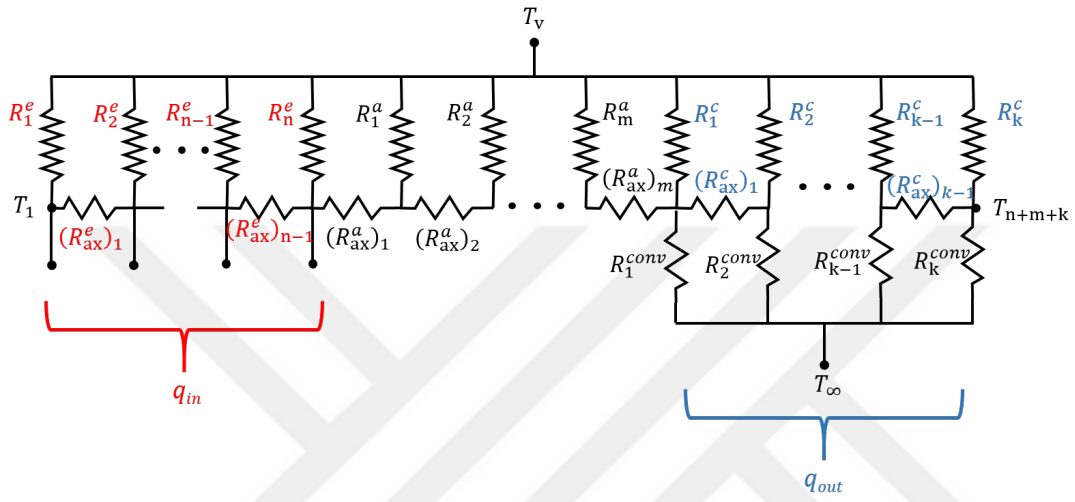

Figure 2.5: Thermal resistance circuit

Nodes given at the thermal resistance circuit are the nodes on the substrate on which the wick is placed. There are some interior nodes such as in between the substrate and wick or interface temperature. The evaporator section is divided into n slices, the adiabatic section into m slices, and the condenser section into k slices. Superscripts within each resistance correspond to the section which the resistance belongs to. For evaporator, adiabatic and condenser section; superscript e, a and c are used respectively.

The concepts of evaporator, condenser and adiabatic up until now are defined according to an outside observer. The evaporator is the part where the heat load is applied and the condenser is the part where the heat is discharged. The adiabatic part is the name of the region between these two sections. If we look at this situation from inside the heat pipe, we can only mention about the existence of two sections. The evaporator section is the section where the liquid temperature is higher than the vapor

temperature and liquid evaporation occurs. Condenser section is the section where the liquid temperature is lower than the vapor temperature and vapor condensation occurs. There is only one point where the liquid temperature is equal to the vapor temperature and there is no phase change at that point. There is no adiabatic region in the heat pipe, instead there is an adiabatic point. In this study, the terms evaporator, condenser and adiabatic sections are used to represent the regions where heat load is applied, heat is discharged and region in between them.

A one-dimensional thermal resistance network has been devised to calculate the equivalent resistance in each section for the heat pipe, between the outer wall temperature (T_b) and the vapor temperature (T_v). Width of the slices (w_{hp}) is equal to inner circumference of the heat pipe as given in Eq. 2.17. The thermal resistance model, schematically represented in Fig. 2.6, is given for a slice from the evaporator. The modeling of adiabatic and condenser sections are identical to evaporator except for the slice lengths.

$$w_{hp} = \pi D_i \tag{2.17}$$

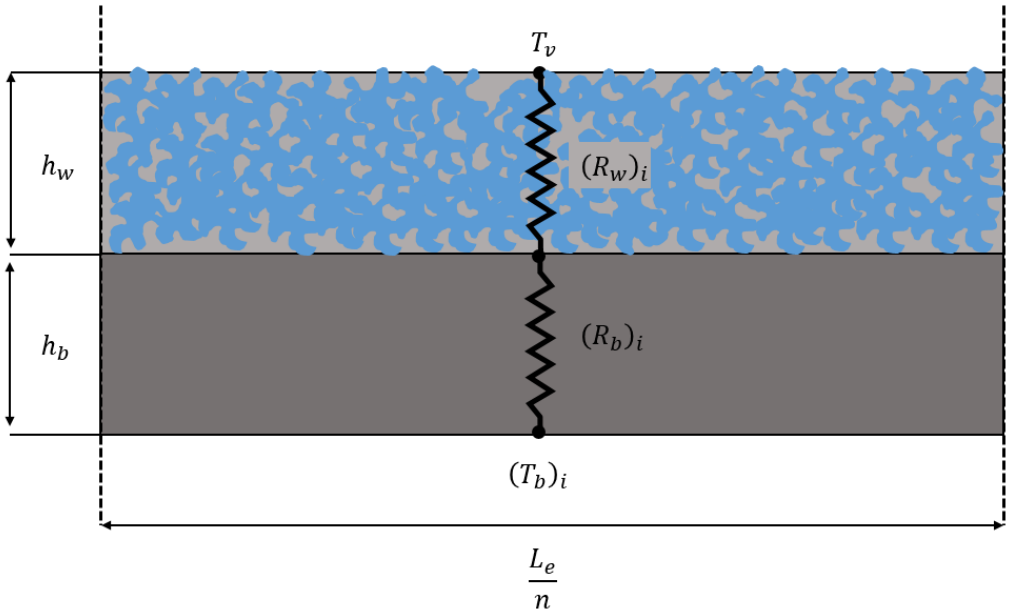

Figure 2.6: Schematic representation of the resistance network

Overall resistance(R_i) at discrete section i from outer wall to vapor temperature for one slice could be expressed as:

$$R_i = R_{b,i} + R_{w,i} \tag{2.18}$$

$R_{b,i}$ is the radial base conduction resistance between outer wall of heat pipe and the beginning of the wick structure. Since all discrete sections are identical in terms of equation, subscript i which denotes the discrete section index, is dropped from now on to the sake of simplicity. $R_{b,i}$ is calculated as follows:

$$R_b = \frac{h_b}{k_s(L_e/n)} \tag{2.19}$$

R_w is the resistance between inner wall of the heat pipe and vapor phase. It consists of two main resistances which are wick conduction resistance and interface resistance.

$$R_w = R_{w,s} + R_{w,int} \tag{2.20}$$

where $R_{w,s}$ stands for wick solid conduction resistance and $R_{w,int}$ is wick-vapor interface resistance. Wick solid conduction resistance is calculated by using wick effective thermal conductivity as,

$$R_{w,s} = \frac{h_w}{k_{eff}(L_e/n)w_{hp}} \tag{2.21}$$

At the top of the wick structure, a thin liquid film occurs inside spherical sections. To calculate the equivalent resistance accurately, a particular interest is given at the interface of liquid-vapor phase. Moreover, as stated before, amorphous cavities at the interface are idealized as a spherical sections filled with liquid. Modelling approach and idealization of this region is illustrated at Fig. 2.7 for hemispheres with cut ratio of 50%. Since the idea behind the modelling of spherical sections is same, below equation are applicable for all other spherical section types.

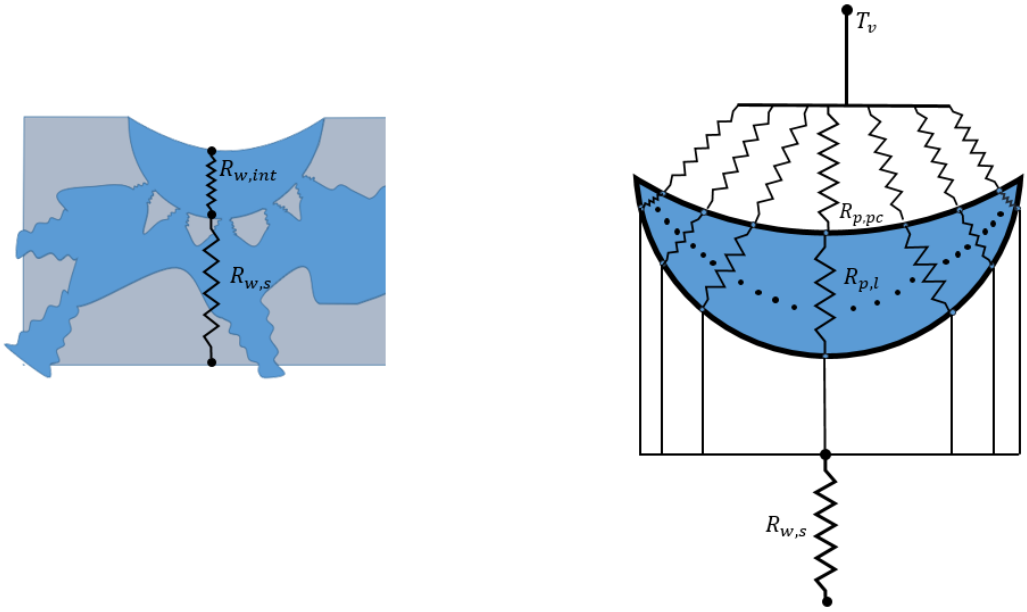

Figure 2.7: Schematic representation and idealization pores

To calculate wick interface resistance $R^f_{w,int}$ for spherical section types, spherical sections are split into finite slices. Two resistances are presented at each slice which are pore liquid $(R_{p,l})^f_g$ and pore phase change resistance $(R_{p,pc})^f_g$ which are defined in Eq. 2.22. One spherical section has number of G slices. Subscript g is the index of slice inside the spherical section. Moreover, as stated before, superscript f is the index of spherical section type.N_f is the number of spherical sections at the solution which has same cut ratio and spherical section type index f.

$$R^f_{w,int} = \frac{1}{N_f}\left[\sum_{g=1}^{G}\frac{1}{(R_{p,l})^f_g + (R_{p,pc})^f_g}\right]^{-1} \tag{2.22}$$

With Eq. 2.22, wick interface resistance for spherical section types are calculated. Moreover, since in a solution domain, there are multiple spherical section types. To find overall wick interface resistance which is combined resistance of all spherical section types could be found as combined them as parallel resistances. Since each solution domain in heat pipe contains F different spherical section types with different cut ratios, overall wick interface resistance could be found as given in Eq. 2.23.

$$R_{w,int} = \left[\sum_{f=1}^{F}\frac{1}{R^f_{w,int}}\right]^{-1} \tag{2.23}$$

First resistance to calculate wick interface resistance $R^f_{w,int}$ is pore liquid resistance $(R_{p,l})^f_g$. Since flow is assumed as laminar and fluid velocity is low, heat transfer within liquid is assumed as pure conduction and any convection within spherical sections is negligible. So, conduction resistance is becomes:

$$(R_{p,l})^f_g = \frac{L^f_g}{(A_{ave})^f_g k_l} \tag{2.24}$$

where, $(A_{ave})^f_g$ is average conduction area between spherical section and interface surface at slice g, k_l is liquid conductivity and L^f_g is the distance between spherical section surface and liquid surfaces at that slice of spherical section.

Second resistance which occurs inside pore region is phase change resistance. It is calculated from kinetic theory by using evaporating mass flux at the interface which it given in Eq. 2.25.

$$m_e{}'' = a(T_{lv} - T_v) + b(P_l - P_v) \tag{2.25}$$

where

$$a = \frac{2\hat{\sigma}}{2 - \hat{\sigma}} \left(\frac{M}{2\pi R_u T_{lv}}\right)^{1/2} \left(\frac{M P_v h_{lv}}{R_u T_{lv} T_v}\right) \tag{2.26}$$

$$b = \frac{2\hat{\sigma}}{2 - \hat{\sigma}} \left(\frac{M}{2\pi R_u T_{lv}}\right)^{1/2} \left(\frac{P_v V_l}{R_u T_{lv}}\right) \tag{2.27}$$

Evaporating mass flux rate due to pressure difference term is negligible with respect to temperature difference. Moreover, evaporation mass flux could be calculated as follows:

$$m_e{}'' = \frac{Q}{h_{fg} A_n} \tag{2.28}$$

where, A_n is evaporation area which is obtained by each slice length around the center axis of spherical section. By combining Eq. 2.25 and 2.28, pore phase change resistance $(R_{p,pc})^f_g$ is obtained as:

$$(R_{p,pc})^f_g = \frac{1}{a h_{fg} A_n} \tag{2.29}$$

The overall thermal resistance network circuit explaning how radial resistance of a slice (R^e_i) is calculated thorough sub-resistances is provided through Fig. 2.8– Fig. 2.10

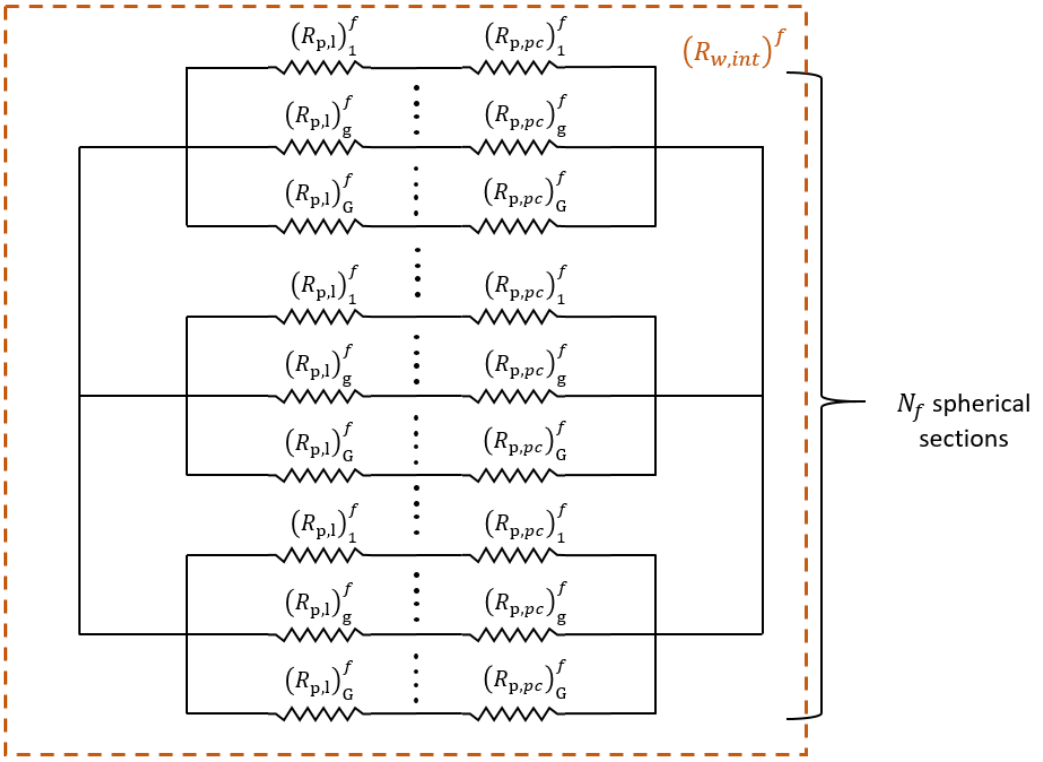

Figure 2.8: Thermal resistance network of wick interface resistance for one spherical section type

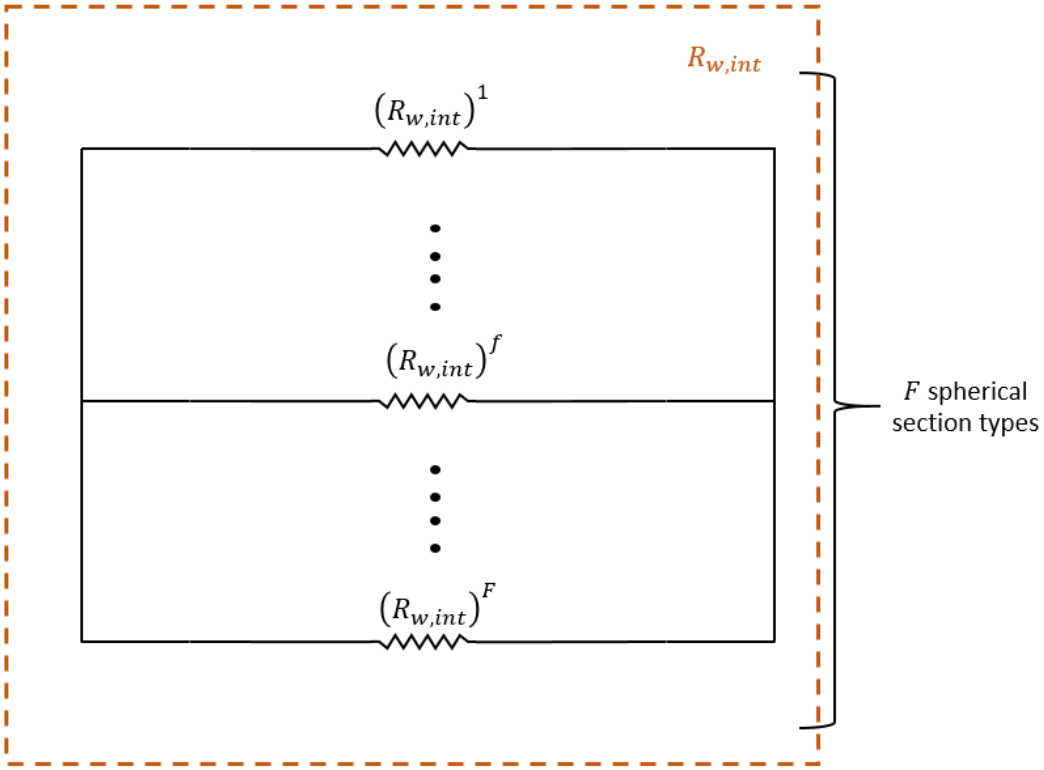

Figure 2.9: Thermal resistance network of wick interface resistance for all spherical sections

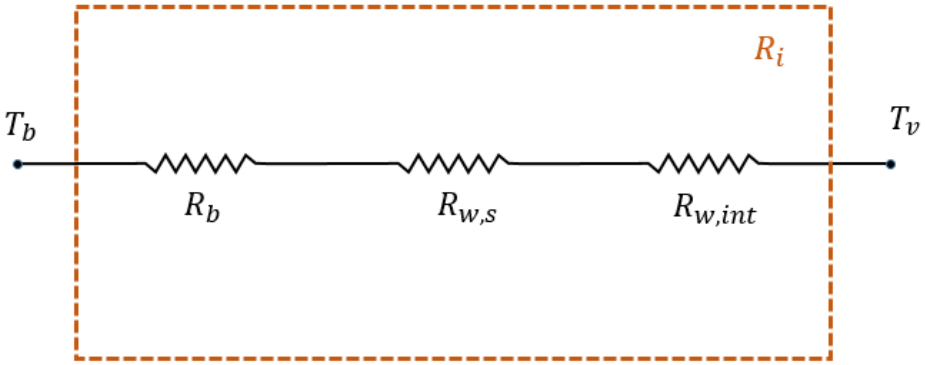

Figure 2.10: Overall thermal resistance network of a slice

CHAPTER 3

RESULTS

3.1 Numerical Model Comparison

This section covers the validation studies conducted for the developed model. The developed model is capable of calculating wall temperatures, vapor phase pressure and temperature as well as the liquid phase pressure distribution. Moreover, radius of curvature and contact angle are calculated for each slice of heat pipe. To demonstrate the accuracy of the model, comparisons have been made with similar studies. As there is no single study in the literature where all these results can be compared, pressure and temperature comparisons have been conducted using two separate studies. However, since the studies did not provide a distribution along the heat pipe for radius of curvature and contact angle, the outputs of these two model parameters have not been validated explicitly.

3.1.1 Flow Model

Tournier and El-Genk [1] developed a 2D transient analysis model to simulate porous wick heat pipes. Moreover, they validated the model through experiments. Thus, in order to validate present model in terms of liquid pressure distribution, vapor pressure and mass flow rate of the heat pipe, Tournier and El-Genk's study is used. Boundary conditions, heat pipe and wick specifications are taken from the benchmark study are summarized at Table 3.1.

Table 3.1: Flow Model Validation Study Parameters in [1]

Parameter	**Value**
Wick Type	Screen Mesh
Wick Permeability (K)	$1.5 \times 10^{-9}\,\mathrm{m}^2$
Wick Porosity (ϵ)	0.5
Wire Radius (R_{wire})	$54\,\mu\mathrm{m}$
Working Fluid	Water
Heat Load	$455\,\mathrm{W}$
Coolant Water Temp.	$295\,\mathrm{K}$
Evaporator Length (L_e)	$600\,\mathrm{mm}$
Adiabatic Length (L_a)	$90\,\mathrm{mm}$
Condenser Length (L_c)	$200\,\mathrm{mm}$
Base Thickness (h_b)	$1.00\,\mathrm{mm}$
Wick Thickness (h_w)	$0.75\,\mathrm{mm}$

In the benchmark study, the vapor temperature and pressure distribution have also been calculated in transient regime. However, steady-state distributions of both vapor and liquid pressure, and mass flow rate of heat pipe are given at the study. In Fig. 3.1, pressure distribution inside wick region is compared. To compare, 5 different number of spherical section types are created which are 1,3,11,31 and 101. In these spherical section types, one spherical section has always been set as a perfect hemisphere and the remaining cut ratios of spherical sections are chosen to be linearly distributed between 0 and 100. For example, 1 spherical section type means a cut ratio of 50% whereas 3 spherical section type has sections with cut ratios of 25%,50% and 75%.

The results of the present model show a high degree of concordance with those of the reference study, as illustrated in the figure. Since the pressure value and therefore the pressure distribution in the evaporator section depends on the initial contact angle, it is expected that the pressure values will be different. For this reason, instead of looking at the absolute pressure value, it would be more accurate to look at the pressure difference between the end of the evaporator and the beginning of the condenser. Liquid and vapor pressure drops, vapor saturation temperature, vapor saturation pressure

and mass flow rates for flow model comparison are given at Table 3.2.

As it could be observed, simulations using all different number of spherical sections nearly have same pressure drop and lower than the comparison study. The primary reason for this is that in the reference study, the pressure drop within the wick is calculated using the Forchheimer equation. The Forchheimer equation contains an additional term compared to the Darcy equation used in the present model, resulting in a higher pressure drop. Nevertheless, it is observed that the difference between the two is relatively small and given on Table 3.2.

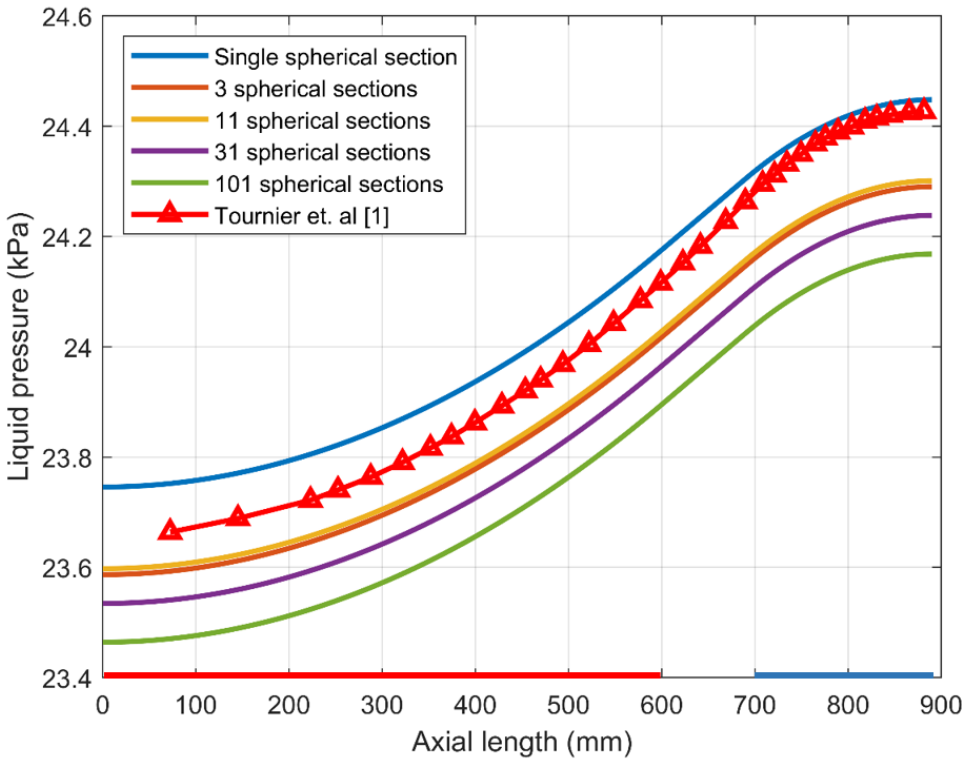

Figure 3.1: Axial variation of liquid pressure

As mentioned earlier, current study assumes that the vapor pressure drop is much smaller and negligible compared to the liquid pressure loss.This can be verified from the referenced study. As seen in the table, the vapor pressure loss corresponds to 0.6% of total pressure drop. Hence, vapor pressure drop is negligible compared to the pressure loss in the liquid.

Table 3.2: Flow Model Comparison of [1] and Current Study

		ΔP_l (Pa)	ΔP_v (Pa)
	[1]	760	4.5
# of spherical sections	1 Cut	704	-
	3 Cut	703	-
	11 Cut	703	-
	31 Cut	702	-
	101 Cut	702	-

Table 3.2 is given for different number of spherical sections. 1 cut stands for structured hemispherical sections with cut percentage of %50. Multiple spherical section type studies are done with equal increment cut percentages. It is observed that number of spherical sections does not have a major impact on pressure drop. Moreover, difference between reference study and present model is reasonably small.

3.1.2 Thermal Model

For heat pipes, two primary performance parameters are crucial: first, the capacity to transport maximum heat load, and second, the maintenance of a minimal temperature difference between the evaporator and condenser. These parameters collectively determine the effectiveness and efficiency of heat transfer within the heat pipe system, essential for various thermal management applications.

In order to compare the thermal model, it is tested with two different studies. First study is to compare thermal model is the experimental study by Huang *et al.* [10]. Moreover, Tournier and El-Genk [1] used the same study to validate their results as well. Parameters of study are already given in Table 3.2. In the experiment, water cooling jacket is used to reject heat from the condenser part of the heat pipe. The cooling water enters the condenser cooling jacket at 294.5 K and with a mass flow rate of 11.33 g/s. At steady-state, heat transfer coefficient between cooling water and condenser is calculated as 1800 $\mathrm{Wm^{-2}K^{-1}}$.

As it could be observed from Fig. 3.2, wall temperature distributions in axial direction

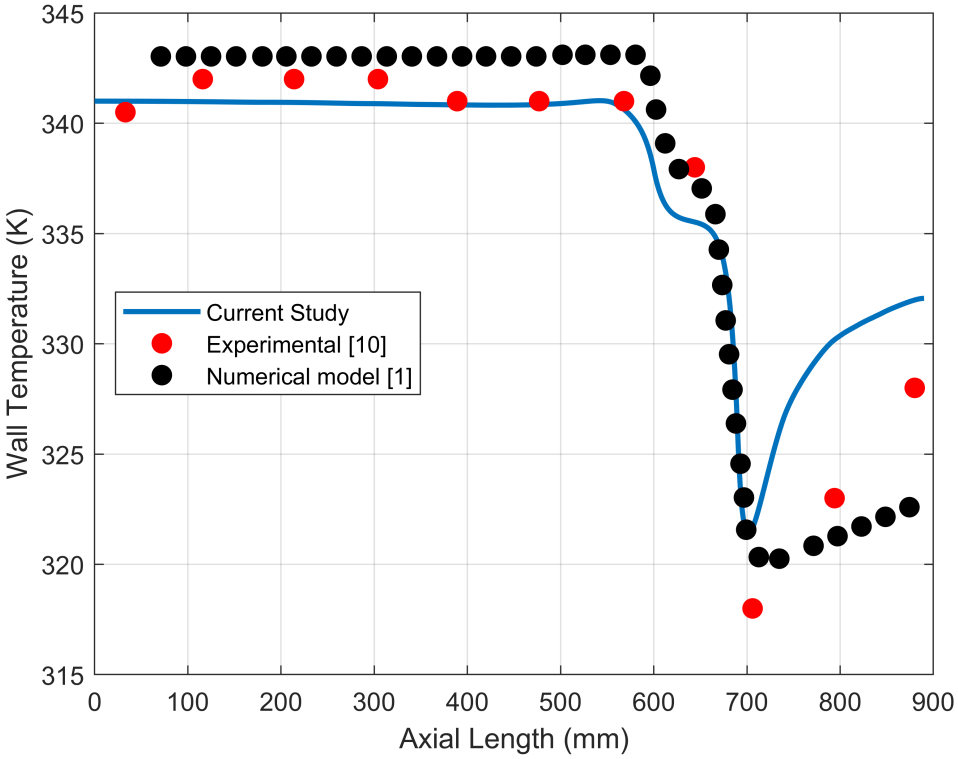

Figure 3.2: Wall temperature distribution validation with [10] and [1]

are similar to each other. However, for both present study and numerical study given in [1] have deviations from the experimental data. The reason for this phenomenon can be attributed to the experimental study providing only the wire diameter for the screen mesh wick, while neglecting to specify the size of the cavities at the interface. Nevertheless, upon examining the behavior of the wall temperature distribution, it can be inferred that the experimental study and the present study exhibit considerable similarity.

Second study to compare is a sintered wick vapor chamber. In their study, Ranjan *et al.* [2] developed a model to calculate wall temperatures for a flat heat pipes. The study is conducted in a 2D model for unit length. A representative sketch of the reference study flat heat pipe is given in Fig. 3.3. As it could be seen, flat heat pipe dimensions and boundary conditions are symmetric. Thus, only half of the flat heat pipe is considered in the present study. Operational conditions and heat pipe specifications which are used in the thermal model comparison study are provided in

Table 3.3. In order to compare thermal model of the current study, same parameters and operational conditions are used. Head load is applied from a length of 2.5 mm on evaporator. To compare, 5 different number of spherical section type are created which are 1, 3, 11, 31 and 101 same as stated in 3.1.1. Result of the comparison is given in Fig. 3.4 and Fig. 3.5.

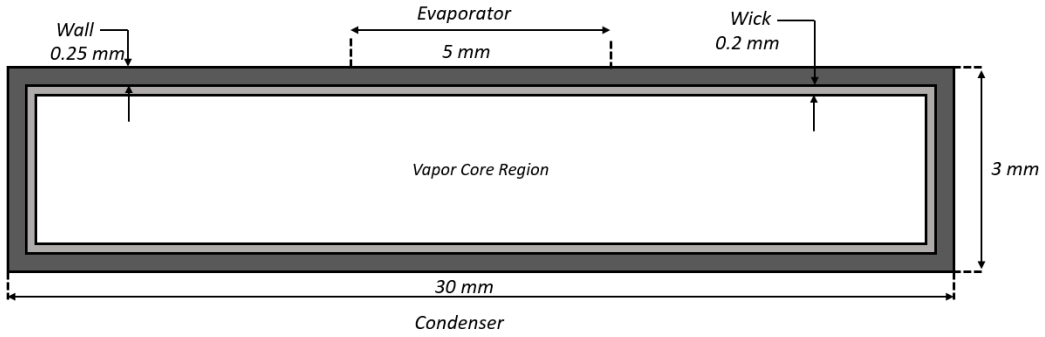

Figure 3.3: Schematic diagram of flat heat pipe of reference study

Table 3.3: Thermal Model Validation Study Parameters in [2]

Parameter	**Value**
Wick Type	Screen Mesh
Wick Permeability (K)	$1.5 \times 10^{-9}\,\mathrm{m}^2$
Wick Porosity (ϵ)	0.56
Pore Radius (R_p)	$10\,\mu\mathrm{m}$
Working Fluid	Water
Wall Material	Copper
Heat Flux	$10\,\mathrm{W\,cm}^{-2}$
Coolant Water Temp.	$298\,\mathrm{K}$
Evaporator Length (L_e)	$5\,\mathrm{mm}$
Adiabatic Length (L_a)	$31\,\mathrm{mm}$
Condenser Length (L_c)	$30\,\mathrm{mm}$
Base Thickness (h_b)	$0.25\,\mathrm{mm}$
Wick Thickness (h_w)	$0.2\,\mathrm{mm}$

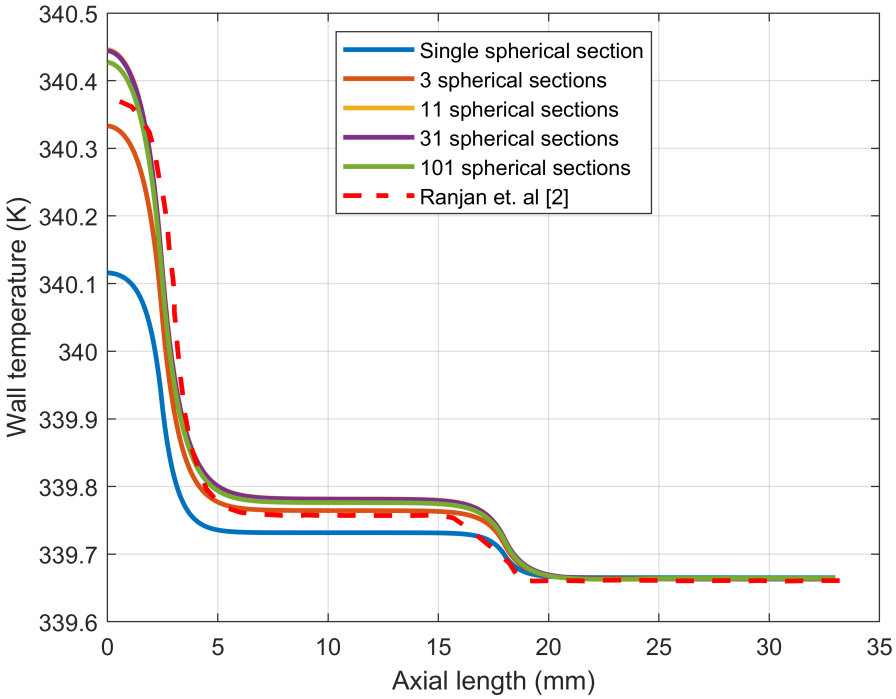

Figure 3.4: Wall temperature distribution comparison at $10\ \mathrm{W/cm^2}$

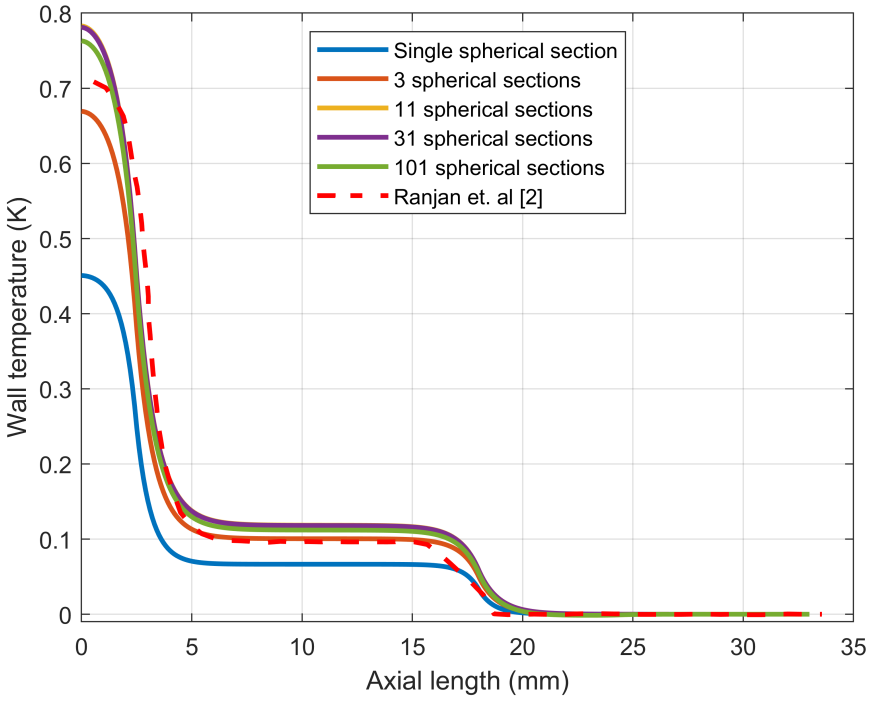

Figure 3.5: Wall temperature difference comparison at $10\ \mathrm{W/cm^2}$

As it could be observed from Fig. 3.4 and Fig. 3.5 as the number of spherical sections increases wall temperature converges to the same value. After 31 spherical sections, difference between 31 and 101 spherical sections is negligible. So, further studies cover spherical sections up to 101 spherical sections. In the benchmark study the temperature difference between evaporator and condenser section is calculated as 0.71 K where current study for 101 spherical sections calculated it as 0.78 K. Thus, relative error between reference study and current study is around 9%. Since the reference model accounts vapor flow and vapor temperature distribution, the difference between reference study and current study is accepted as reasonable.

Moreover, it is seen that temperature difference for one spherical section which is a perfect hemisphere is lower than the 101 spherical sections. It means that the temperature difference between two ends is lower, which is a favorable parameter for a heat pipe, if amorphous cavities are perfect hemispheres instead of random shapes.

3.2 Effect of Pore Radius on Thermal Performance

In this section, the relationship between the thermal performance in sintered heat pipes and the pore radius is investigated. To investigate relationship between pore radius and thermal performance of a heat pipe, two different batch study are constructed. Temperature difference at a constant heat load and maximum heat load for altering pore radius are investigated. The geometric and operational parameters provided for sintered heat pipes in Table 3.4 are used for simulations. Cavities at the interface are simulated for 101 spherical sections with equal increment cut percentages.

The first parameter under investigation is the pore radius effect on the maximum heat load that could be transported. For simulations, the pore radius range is selected to be between 1 μm and 250 μm. The maximum heat load corresponding to each pore radius has been calculated. As heat load increases contact angle at each spherical sections decreases. Whenever contact angle reaches the material contact angle, it could be concluded that dry-out occurs for that specific spherical section. In other words, the spherical section type become non-functional whenever the contact angle

becomes lower than the material contact angle.

As it is expected, percentage of non-functional spherical sections are at its maximum value at the end of the evaporator and its minimum value at the beginning of condenser section. Maximum heat load is determined as whenever percentage of non-functional spherical sections are over 80%. The relationship between pore radius and the maximum heat load heat pipe could carry is illustrated in Fig.3.6.

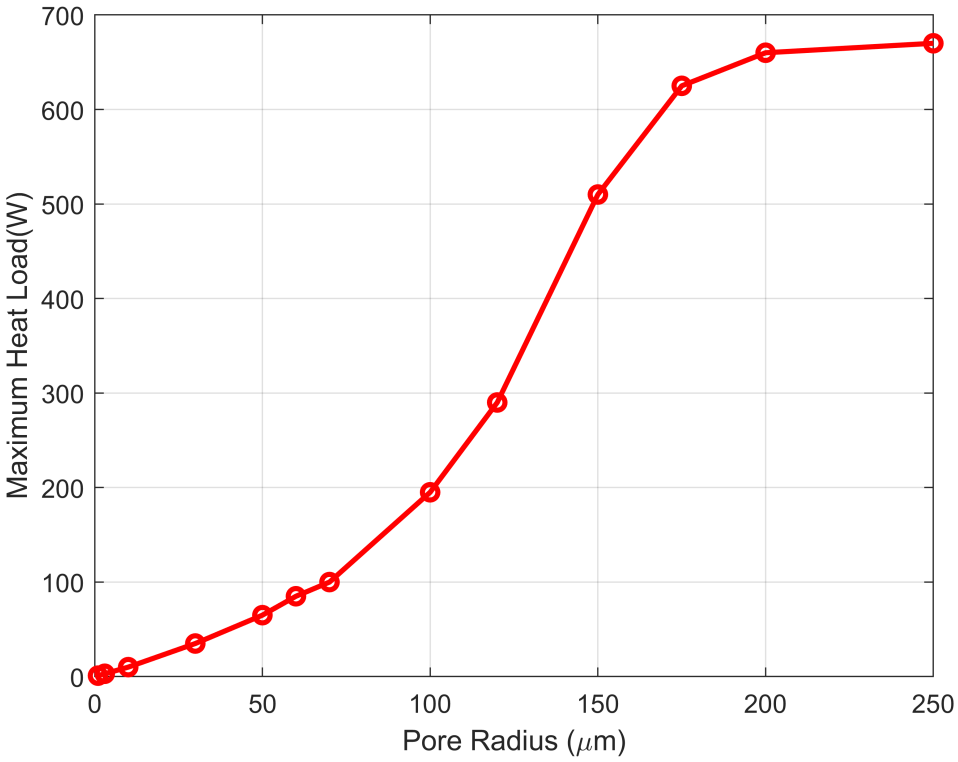

Figure 3.6: Pore radius effect on maximum heat load

As it could be observed from Fig. 3.6 as the pore radius increases maximum heat load that heat pipe could transport also increases. At smaller pore radius, increment in radius results in higher maximum heat load increments. On the other hand, after some point, pore radius effect on maximum heat load becomes weaker. To better understand the behavior, one could examine the ranges between 100 µm – 150 µm and 200 µm – 250 µm. In the first range 50 µm increase in pore radius results in 300 W maximum heat load capacity. On the other hand for the second range, 50 µm increase in pore radius results in 40 W maximum heat load capacity.

Fig. 3.7 illustrates percentage of non-functional pore types along heat pipe for various heat loads. As expected, percentage of non-functional pore types is at its maximum at the end of evaporator. Through condenser, more spherical section types become functional as contact angle increases. At the beginning of the condenser, surface shape at the interface becomes flat since vapor pressure and liquid pressure become nearly equal to each other. So, regardless of heat load, all non-functioning pore types converge to the same value which is a physical limit.

Moreover, in Fig. 3.8, it could be observed that the temperature difference and percentage of non-functional pore types at the end of the evaporator increases as heat load increases. Percentage of increment in heat load results in lower contact angle, hence increment in non-functional pore types. Therefore the temperature difference increases. Similar plots for 10 μm, 60 μm and 250 μm are given at Fig. 3.9–3.14.

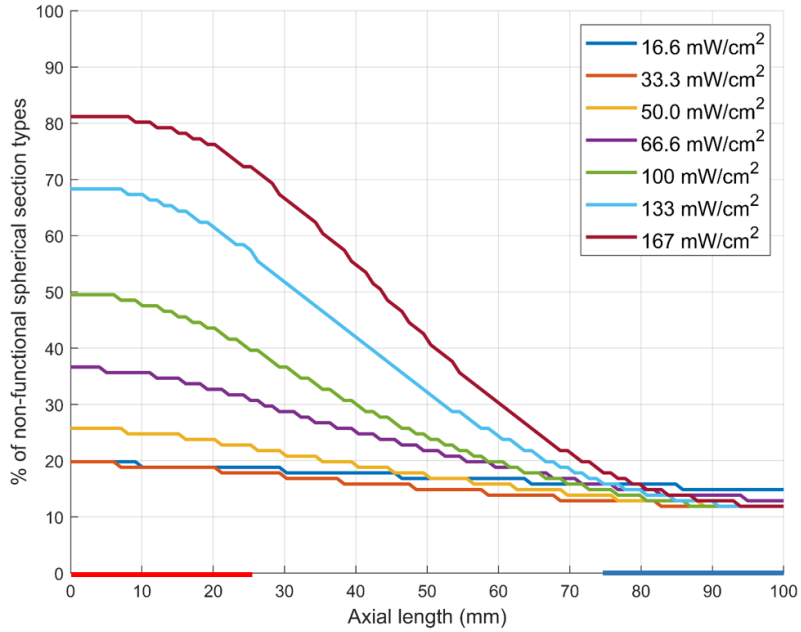

Figure 3.7: Non-functional spherical section types along heat pipe for various heat loads for 1.0 µm pore size

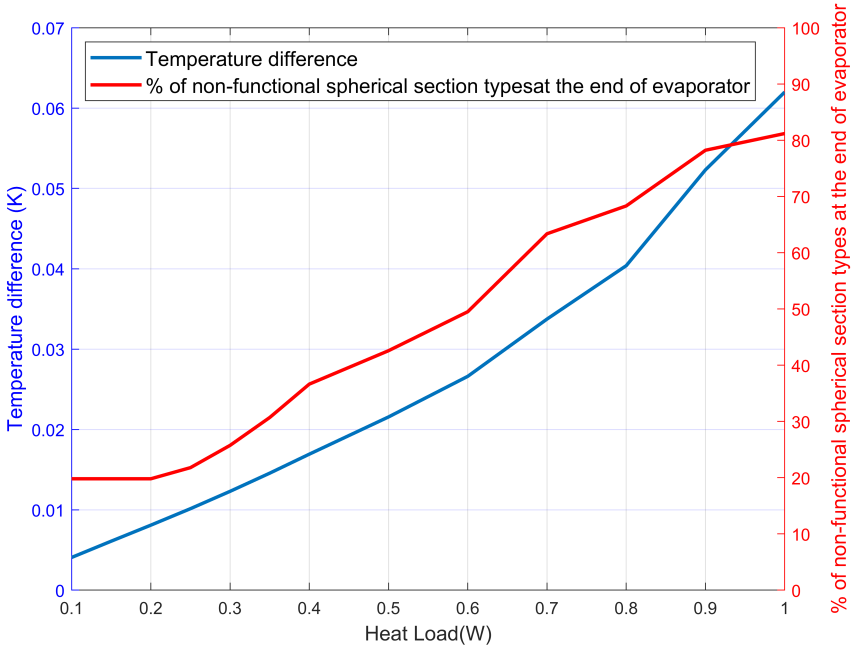

Figure 3.8: Non-functional spherical section types at the end of evaporator and temperature difference between two ends for various heat loads for 1.0 µm pore size

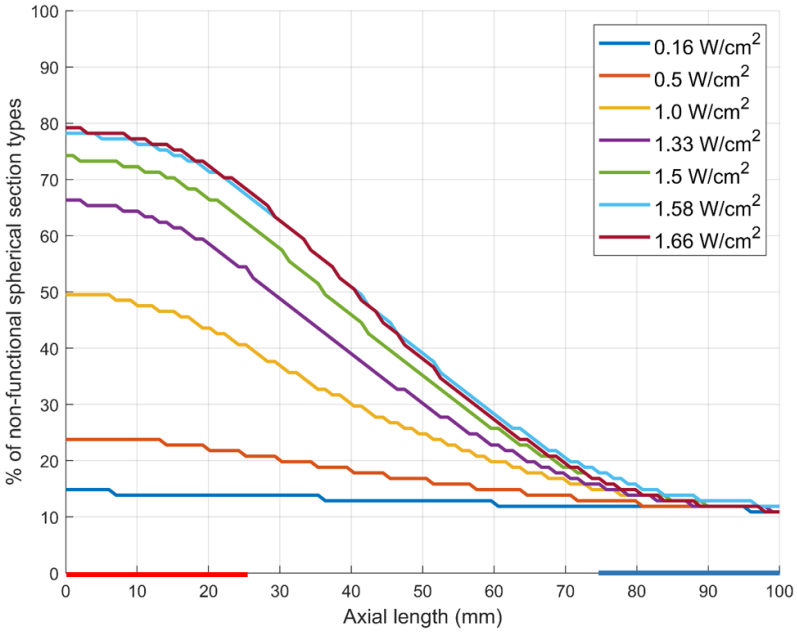

Figure 3.9: Non-functional spherical section types along heat pipe for various heat loads for 10 µm pore size

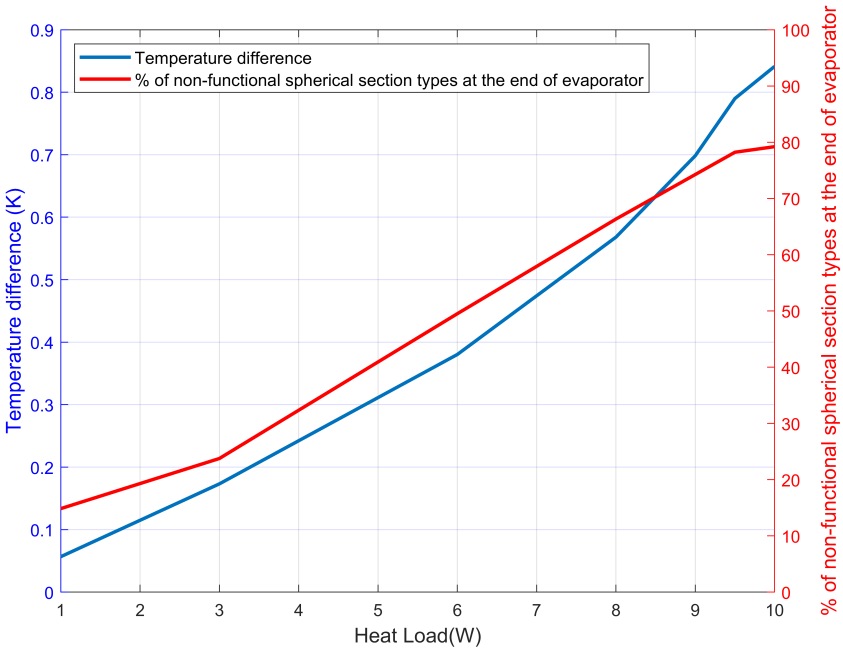

Figure 3.10: Non-functional spherical section types at the end of evaporator and temperature difference between two ends for various heat loads for 10 µm pore size

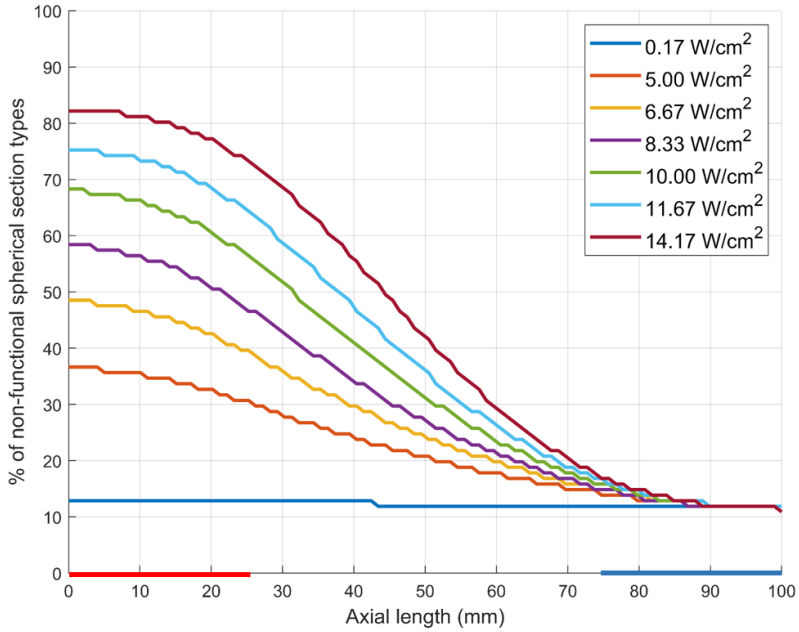

Figure 3.11: Non-functional spherical section types along heat pipe for various heat loads for 60 µm pore size

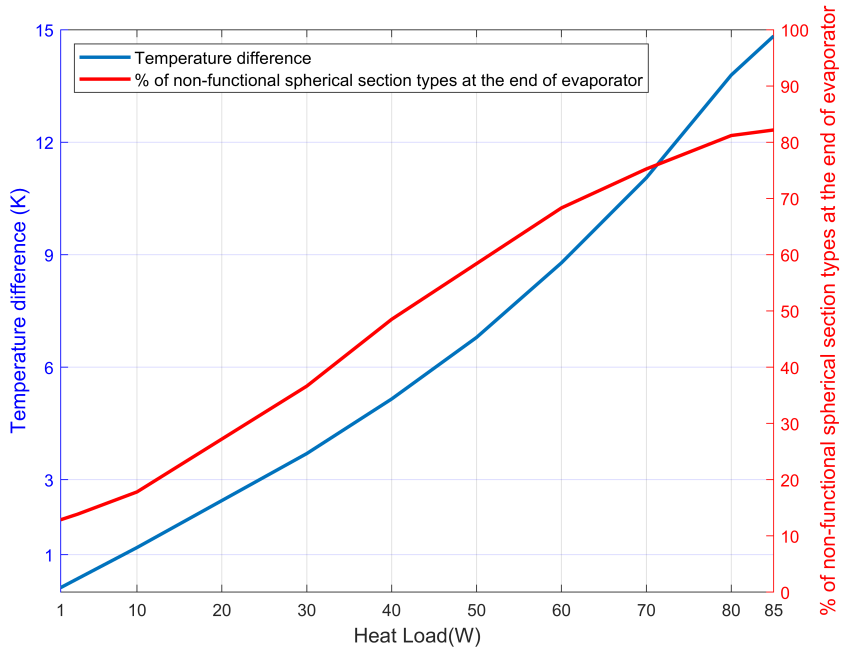

Figure 3.12: Non-functional spherical section types at the end of evaporator and temperature difference between two ends for various heat loads for 60 µm pore size

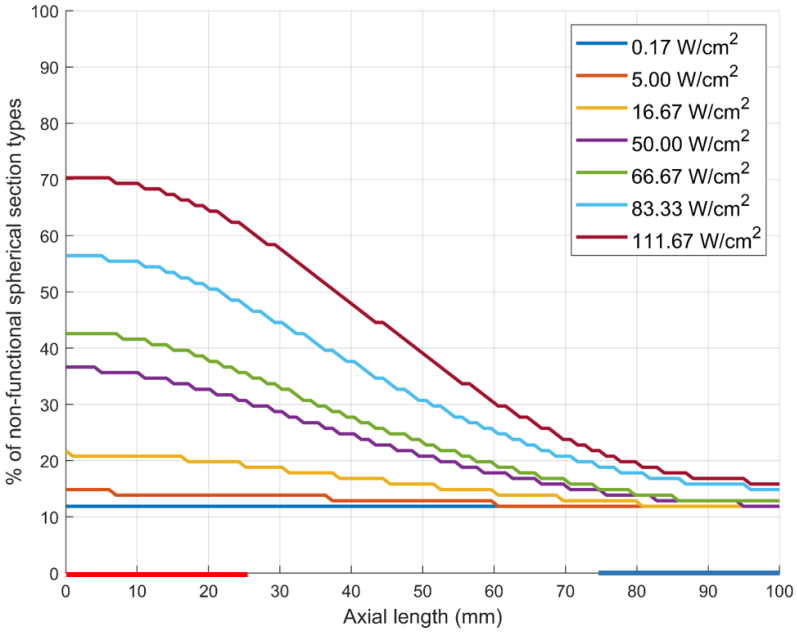

Figure 3.13: Non-functional spherical section types along heat pipe for various heat loads for 250 µm pore size

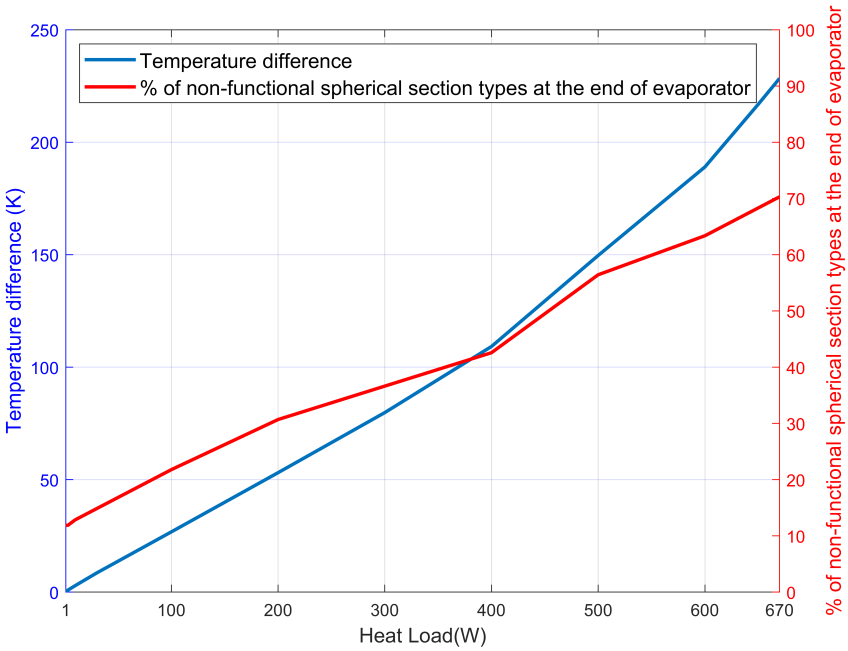

Figure 3.14: Non-functional spherical section types at the end of evaporator and temperature difference between two ends for various heat loads for 250 µm pore size

3.3 Effect of Pore Radius on Temperature Difference

Second parameter investigated is relationship between the temperature difference between evaporator and condenser section with pore radius at given heat load. Heat loads are taken as 1, 10, 30 and 100 W. The pore radius range is selected as in between 1 µm and 250 µm which are available pore radius for sintered wick heat pipes [38]. Moreover, mostly used pore radius range in industry is 25–100 µm. The minimum pore radius shown on the $x-$axis in each plot is the minimum radius that can carry that heat load. Moreover, cavities at the interface are simulated as 101 different spherical section types as before. In plot left ordinate gives the temperature difference between two ends of heat pipe. Moreover, right ordinate denotes the percentage of non-functional spherical sections at the end of the evaporator.

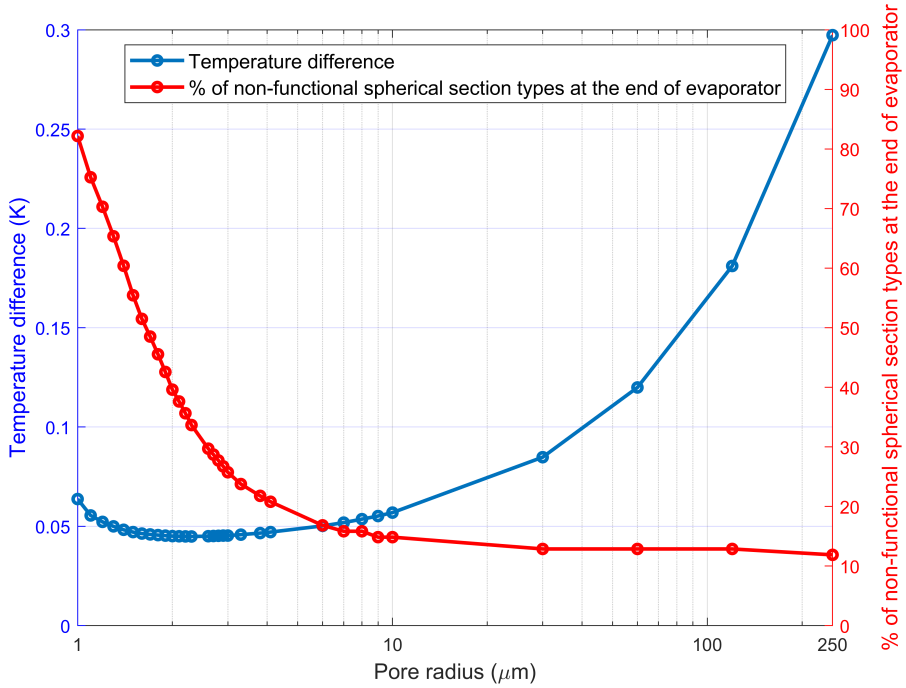

Figure 3.15: Effect of pore radius on temperature difference for $0.16\,\mathrm{W/cm^2}$

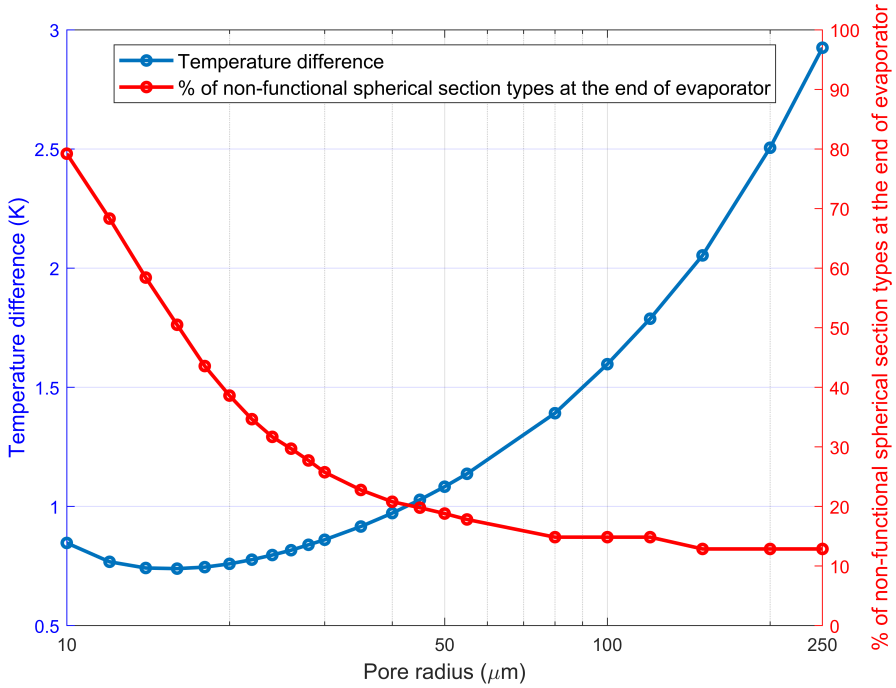

Figure 3.16: Effect of pore radius on temperature differences for $1.6\,\mathrm{W/cm^2}$

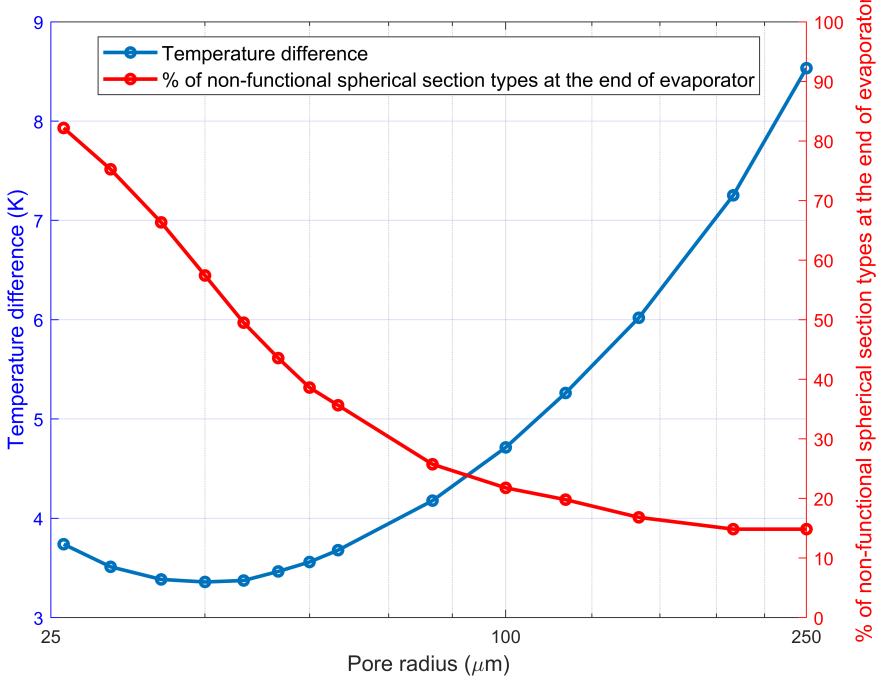

Figure 3.17: Effect of pore radius on temperature difference for $5.0\,\mathrm{W/cm^2}$

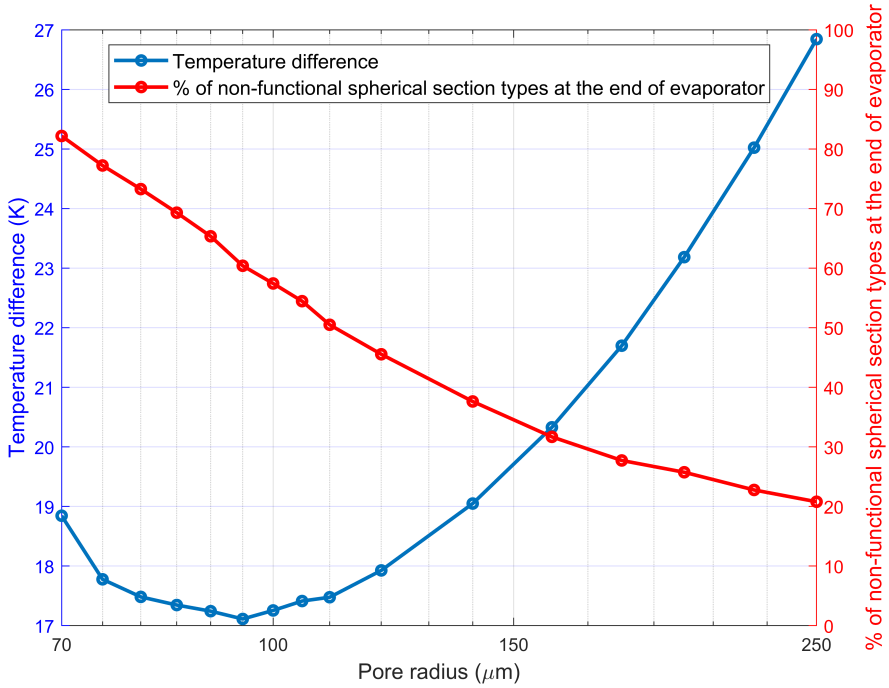

Figure 3.18: Effect of pore radius on temperature difference for $16.6\,\mathrm{W/cm^2}$

In plot of Figs.(3.15 – 3.18), abscissa is given in logarithmic scale to see behavior of relationship better. Increasing the pore radius leads to a decrease in the temperature difference up to a point. To better explain this behavior, percentage of non-functional pore types at the end of the evaporator is given on the left ordinate. The minimum pore radius given in the graph represents the smallest pore radius that can carry that heat load. In the case where the maximum heat load is carried, the non-functioning spherical sections at the end of the evaporator are over 80% of the total spherical section types. As the pore radius of wick increases for a constant heat load, pressure loss of the liquid decreases and apparent contact angle increases. This results in more pore types becoming functional as it could be seen from left ordinate from plots. On the other hand, as the pore radius increases, the film thickness at the interface also increases. After a certain point, the increase in film thickness becomes a more dominant factor. After this point, a further increase in pore radius, results in an increase of temperature difference. Since lower temperature difference is a desirable parameter for heat pipe design, for a certain heat load pore radius should selected higher than the minimum pore radius that could carry that heat load. For example, in Fig. 3.18, for

100 W heat load, pore radius 70 μm has higher temperature difference than 100 μm. Moreover, as pore radius increases maximum heat load increases. So, choosing pore radius of 100 μm rather than 70 μm is advantageous.

3.4 Hypothetical Porous Media with Structured Cavities

In Fig. 3.5, it is observed that one spherical section type has lower temperature difference than 101 spherical section type. However, since sintered wick heat pipes contain amorphous cavities at the interface, 101 spherical section type with different cut ratios is more realistic modeling than the one spherical section type. This section focuses on what would happen if the interface consisted of a single spherical section which is a perfect hemisphere instead of amorphous cavities.

In order to determine the thermal performance, a sintered wick heat pipe with a single spherical section is compared with a sintered wick heat pipe with a number of spherical sections of 101. Moreover, to create a baseline study, performance comparison with flat grooved heat pipes are presented in this section. Grooved heat pipe parameters are directly taken from [3]. The parameters of the sintered wick heat pipes are set such that the two heat pipes have the same net flow area, the same available pressure head, and the same outer diameter. The pore size ensuring the same available pressure head is determined as shown in Fig.3.19. Study parameters are given at Table 3.4.

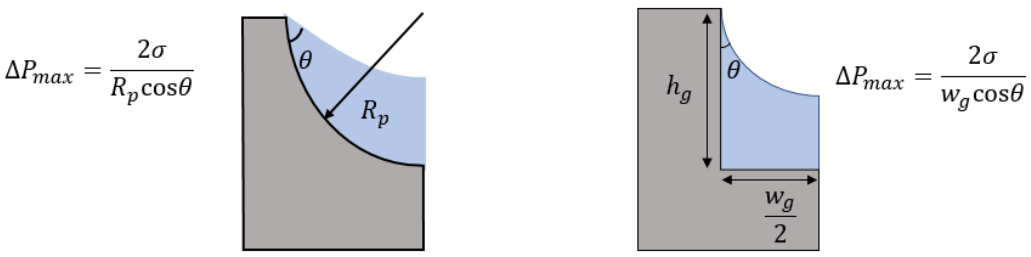

Figure 3.19: Available pressure head in sintered and grooved heat pipes

Table 3.4: Comparison parameters in [3]

Common parameters	Heat Load (W)	9.5
	Evaporator length (mm)	26
	Adiabatic length (mm)	48
	Condenser length (mm)	26
	Wall thickness (mm)	1.6
	Fluid	Water
	Condenser Temperature (K)	283
Groove parameters	Groove width (mm)	0.6
	Groove height (mm)	0.4
Porous wick parameters	Pore radius (mm)	0.6
	Porosity	0.55
	Wick height (mm)	1
	Wick width (mm)	8.3

Pressure drop distribution is given at Fig. 3.20. As it could be observed that, grooved wick has lower pressure drop than sintered wick heat pipes as expected. Pressure drop of hypothetical porous media with structured interface wick is slightly higher than sintered wick with 101 spherical section types. Pressure drop of sintered wick with one spherical section is around 12 Pa whereas grooved heat pipe has 5 Pa pressure drop. Wall temperature comparison are given at Fig. 3.21. It could be observed that, sintered wick heat pipe with 101 spherical section types is operating with higher temperature difference with respect to flat grooved heat pipe (FGHP). On the other hand, hypothetical porous media with structured interface wick has lower temperature drop than other two heat pipes. So, as expected before, if such a wick structure could be manufactured, thermal performance would be better than the FGHP.

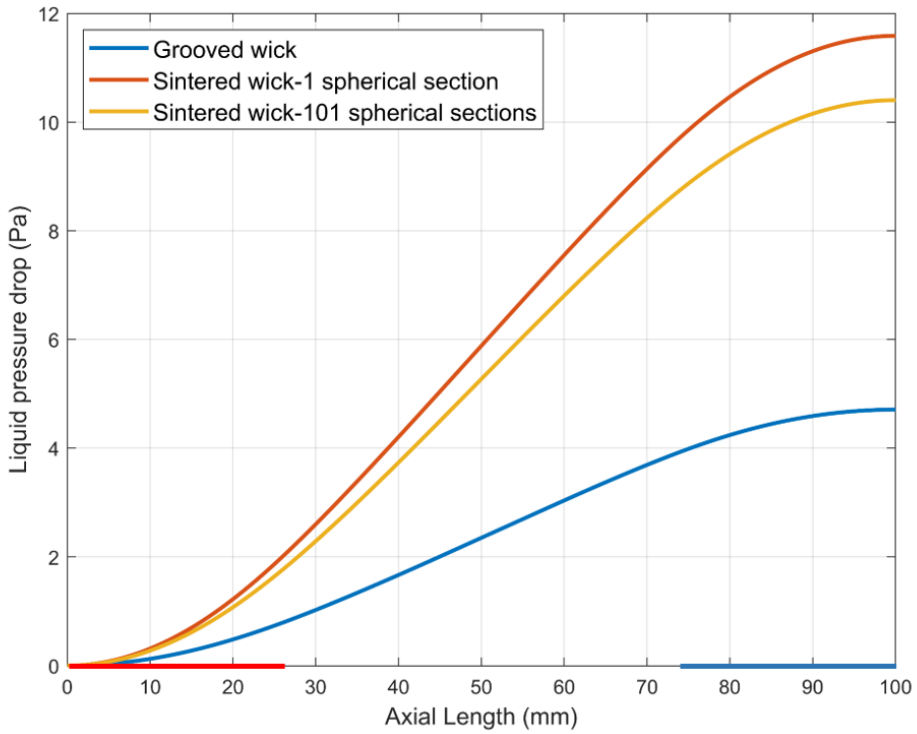

Figure 3.20: Pressure distribution comparison

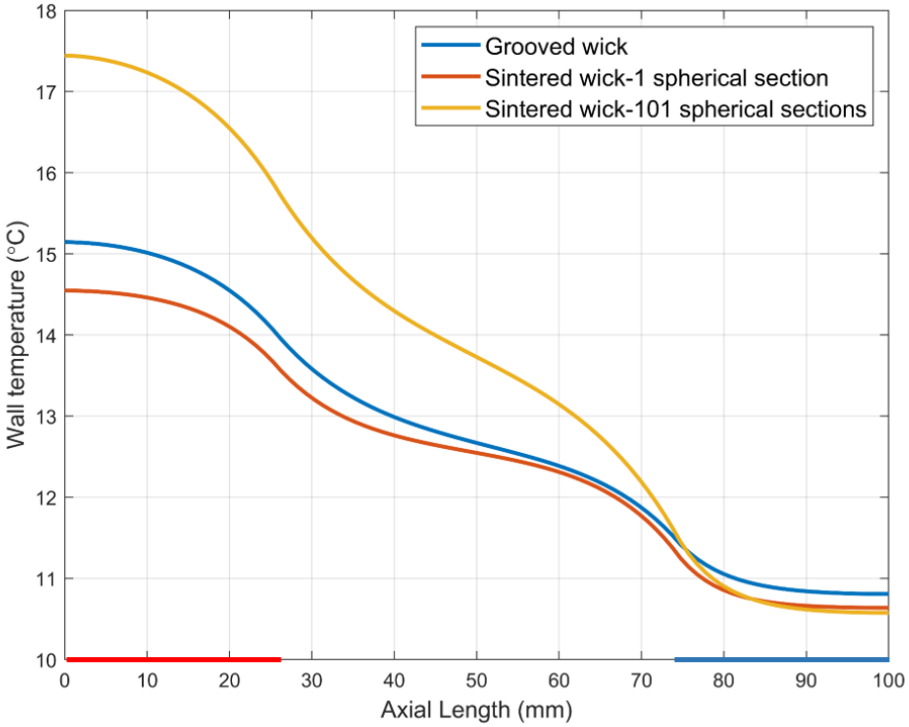

Figure 3.21: Wall temperature comparison

CHAPTER 4

CONCLUSION AND FUTURE WORK

In this thesis study, a thermal resistance network model is used to accurately determine the thermal performance of sintered wick heat pipes by modeling phase change in surface pores. The flow in the sintered wick is modeled as porous medium flow. Porous medium contains amorphous voids both on the interior and on the surface. These voids are usually randomly shaped. For this reason, experimental correlations are usually used to calculate both the pressure drop across the wick and the heat transfer at the interface. In this study, the Darcy porous medium model was used to calculate the pressure drop across the wick and the permeability value for the wick was obtained from experimental correlations. On the other hand, the biggest advantage of the model compared to other studies is that it does not need an effective heat transfer coefficient obtained from experimental correlations when making thermal performance calculations. Instead, amorphous voids at the interface are modeled as a combination of many spherical sections which are cut from certain percentages. These spherical sections are added to the thermal resistance network created.

While the developed model solves the liquid flow in the wick, it assumes that the vapor flow is at constant pressure and temperature. This assumption is supported by comparison with the studies that also solve the vapor flow. In the comparison study for the flow model, a 7% difference in the liquid pressure drop between the reference study and the current study was observed. The main reason for this difference is that the pressure drop model used in the reference study is the Forchheimer model, not the Darcy model. In this case, a slightly higher pressure drop is expected and quite normal. In addition, the reference study also took into account the vapor pressure drop. According to the results, the vapor pressure drop corresponds to 0.5% of the liquid

pressure drop. In the second comparison study, wall temperatures have been compared with the reference study. The results of the existing model and the comparison study are consistent and very well matched.

After the comparison of the model with reference studies, the effect of pore radius on the thermal performance of the heat pipe is investigated. There are two basic performance parameters for a heat pipe. These performance parameters are the maximum heat load that the heat pipe can carry and the temperature difference between two ends while carrying a certain heat load. The conclusions of the study could be summarized as follows:

- In sintered wick heat pipes there exists a dry-out phenomenon that is due to non-functioning spherical sections at every cross-section and load condition. Whenever contact angle at a spherical section attains a value lower than the material contact angle, that specific spherical section type becomes non-functional. As more spherical section types become non-functional, thermal resistance in that cross section increases. As the overall thermal resistance increases, the temperature difference between two ends of heat pipe in effect increases.
- For a given heat load, increasing the pore radius leads to a decrease in the temperature difference, initially. This is due to the decrease in the percentage of non-functional spherical sections as the pore radius increases at the same heat load. However, after a certain point, the temperature difference increases as the pore radius increases. The reason for this is that the effect of increasing thin film thickness becomes more dominant.
- As the pore radius increases, the maximum heat load that the heat pipe can carry also increases. However, the slope of the curve of the graph decreases with increasing pore radius. In other words, as the pore radius increases, the rate of increase of the maximum heat load decreases.
- For a desirable maximum heat load capacity Fig. 3.6 can be taken into account when designing a sintered wick heat pipe using H-PAT to find a pore size interval. After that, to obtain the minimum temperature difference between two ends of the heat pipe, the effect of pore radius on temperature difference plots could be used, such as given in Figs. 3.15–3.18. The minimum temperature

difference at a given heat load is not obtained at the minimum pore radius. The minimum temperature difference is obtained at a value larger than the minimum pore radius. In addition, if the optimum point of the pore radius is larger than the smallest pore radius that can carry the specified heat load, it means that the maximum heat capacity is also higher. For this reason, the given plots should be carefully examined and pore design should be made around the optimum point.

Future studies and some suggestions could be summarized as follows:

- In the study, the number of spherical section types are considered identical for each discrete solution domain along the heat pipe. In future studies, it could be aimed to increase the performance of the heat pipe by changing spherical sections cut percentage along the heat pipe axis to optimize the geometry.
- In the study, it is assumed that each type of spherical section covers the same amount of area at a discrete solution domain. These studies could be repeated using a distribution of pore size. For example, spherical sections with 50% cut ratio could occupy areas larger than spherical sections with 10% cut ratio. With the results obtained from the experiments, it could be compared which modeling approach gives closer results.
- In the current study, only a single pore radius is used along the heat pipe. Future studies could be repeated by multiple pore radius along heat pipe. Pore size distribution in heat pipe could be arrange in linear spacing or Gaussian distribution around an average pore radius.

REFERENCES

[1] J.-M. Tournier and M. El-Genk, "A heat pipe transient analysis model," *International Journal of Heat and Mass Transfer*, vol. 37, no. 5, pp. 753–762, 1994.

[2] R. Ranjan, J. Y. Murthy, S. V. Garimella, and U. Vadakkan, "A numerical model for transport in flat heat pipes considering wick microstructure effects," *International Journal of Heat and Mass Transfer*, vol. 54, no. 1, pp. 153–168, 2011.

[3] S. Saygan, Y. Akkus, Z. Dursunkaya, and B. Cetin, "Capillary boosting for enhanced heat pipe performance through bifurcation of grooves: Numerical assessment and experimental validation," *International Communications in Heat and Mass Transfer*, vol. 137, p. 106162, 2022.

[4] "Heat pipe wick structures exposed: Sintered, groove and mesh." `https://www.frostytech.com/articles/2466/index.html`, November 2009.

[5] B. Xiao and A. Faghri, "A three-dimensional thermal-fluid analysis of flat heat pipes," *International Journal of Heat and Mass Transfer*, vol. 51, no. 11, pp. 3113–3126, 2008.

[6] Y. Maydanik, "Loop heat pipes," *Applied Thermal Engineering*, vol. 25, no. 5, pp. 635–657, 2005.

[7] C. Tarau, W. Anderson, and C. Peters, "Thermal management system for long-lived venus landers," 07 2011.

[8] C. Dave, P. Dandale, K. Shrivastava, D. Dhaygude, K. Rahangdale, and N. More, "A review on pulsating heat pipes: Latest research, applications and future scope," *Journal of Thermal Engineering*, vol. 7, pp. 387–408, 02 2021.

[9] B. Zohuri, *Heat Pipe Theory and Modeling*, pp. 43–166. Cham: Springer International Publishing, 2016.

[10] L. Huang, M. El-Genk, and J.-M. Tournier, "Transient performance of an inclined water heat pipe with a screen wick," vol. 236, pp. 87–92, 01 1993.

[11] G. E. Moore, "Cramming more components onto integrated circuits, reprinted from electronics, volume 38, number 8, april 19, 1965, pp.114 ff.," *IEEE Solid-State Circuits Society Newsletter*, vol. 11, no. 3, pp. 33–35, 2006.

[12] S. Electronics., "Samsung foundry innovations power the future of big data, ai/ml and smart, connected devices." Samsung Newsroom, October 2021.

[13] S. Electronics., "Samsung starts industry's first mass production of system-on-chip with 10-nanometer finfet technology." Samsung Newsroom, October 2016.

[14] S. Sohel Murshed and C. Nieto de Castro, "A critical review of traditional and emerging techniques and fluids for electronics cooling," *Renewable and Sustainable Energy Reviews*, vol. 78, pp. 821–833, 2017.

[15] U. D. of Defense, *MIL-HDBK-217F, MILITARY HANDBOOK: RELIABILITY PREDICTION OF ELECTRONIC EQUIPMENT*. U.S Department of Defense, Washington DC, USA, 1991.

[16] A. Uysal, A. Keçebaş, and M. Kayfeci, "Chapter 32 - futuristic methods of electronics cooling," in *Handbook of Thermal Management Systems* (F. Aloui, E. G. Varuvel, and A. Sonthalia, eds.), pp. 687–702, Elsevier, 2023.

[17] B. Lautrup, *Surface Tension*. CRC Press, 2019.

[18] D. Reay, P. Kew, and R. McGlen, "Chapter 2 - heat transfer and fluid flow theory," in *Heat Pipes (Sixth Edition)* (D. Reay, P. Kew, and R. McGlen, eds.), pp. 15–64, Oxford: Butterworth-Heinemann, sixth edition ed., 2014.

[19] P. Nemec, A. Čaja, and M. Malcho, "Mathematical model for heat transfer limitations of heat pipe," *Mathematical and Computer Modelling*, vol. 57, no. 1, pp. 126–136, 2013. Mathematical and Computer Modelling in Power Control and Optimization.

[20] G. P. Peterson and B. K. Bage, "Entrainment Limitations in Thermosyphons and Heat Pipes," *Journal of Energy Resources Technology*, vol. 113, pp. 147–153, 09 1991.

[21] B. Kim and G. Peterson, "Analysis of the critical weber number at the onset of liquid entrainment in capillary-driven heat pipes," *International Journal of Heat and Mass Transfer*, vol. 38, no. 8, pp. 1427–1442, 1995.

[22] H. Darcy, *Les Fontaines Publiques de la Ville de Dijon*. CRC Press, 1856.

[23] A. Hazen, "Some physical properties of sands and gravels, with special reference to their use in filtration," 1893.

[24] M.Muskat, *The Flow of Homogeneous Fluids Through Porous Media*. McGraw Hill, 1937.

[25] E.Krüger, *Internationale Mitteilungen fur Bodenkunde*. 1918.

[26] Forchheimer, "Wasserbewegung durch boden," *Zeitschrift des Vereins deutscher Ingenieure*, 1901.

[27] M. Ababneh, F. M. Gerner, P. Chamarthy, P. de Bock, S. S. Chauhan, and T. Deng, "Thermal-fluid modeling for high thermal conductivity heat pipe thermal ground planes," *Journal of Thermophysics and Heat Transfer*, vol. 28, pp. 270–278, 2014.

[28] U. Vadakkan, S. V. Garimella, and J. Y. Murthy, "Transport in Flat Heat Pipes at High Heat Fluxes From Multiple Discrete Sources ," *Journal of Heat Transfer*, vol. 126, pp. 347–354, 06 2004.

[29] K. Zeghari and H. Louahlia, "Flat miniature heat pipe with sintered porous wick structure: experimental and mathematical studies," *International Journal of Heat and Mass Transfer*, vol. 158, p. 120021, 2020.

[30] G. Odabaşı, *Modeling of Multidimensional Heat Transfer in a Rectangular Grooved Heat Pipe*. Phd thesis, Middle East Technical University, June 2014.

[31] Y. S. Li, H. F. He, and Z. X. Zeng, "Evaporation and condensation heat transfer in a heat pipe with a sintered-grooved composite wick," *Applied Thermal Engineering*, vol. 50, pp. 342–351, 2013.

[32] C. Ferrandi, F. Iorizzo, M. Mameli, S. Zinna, and M. Marengo, "Lumped parameter model of sintered heat pipe: Transient numerical analysis and validation," *Applied Thermal Engineering*, vol. 50, no. 1, pp. 1280–1290, 2013.

[33] B. Ch Nookaraju, P. Kurma Rao, and S. Naga Sarada, "Experimental and numerical investigation on enhancement in thermal characteristics of sintered copper wick heat pipe using deionized water as fluid," *Materials Today: Proceedings*, vol. 4, no. 2, Part A, pp. 1321–1331, 2017. 5th International Conference of Materials Processing and Characterization (ICMPC 2016).

[34] K. Zeghari, H. Louahlia, and S. Le Masson, "Experimental investigation of flat

porous heat pipe for cooling TV box electronic chips," *Applied Thermal Engineering*, vol. 163, p. 114267, 2019.

[35] M. Zhu, J. Huang, M. Song, and Y. Hu, "Thermal performance of a thin flat heat pipe with grooved porous structure," *Applied Thermal Engineering*, vol. 173, p. 115215, 2020.

[36] N. Sangpab, P. Sakulchangsatjatai, N. Kammuang-lue, and P. Terdtoon, "Mathematical model of bent-flattened sintered-grooved heat pipe with concept of receding-and-excessing fluid," *Case Studies in Thermal Engineering*, vol. 27, p. 101307, 2021.

[37] S. Zhang, C. Chen, G. Chen, Y. Sun, Y. Tang, and Z. Wang, "Capillary performance characterization of porous sintered stainless steel powder wicks for stainless steel heat pipes," *International Communications in Heat and Mass Transfer*, vol. 116, p. 104702, 2020.

[38] Y.-Y. Tsai and C.-H. Lee, "Effects of sintered structural parameters on reducing the superheat level in heat pipe evaporators," *International Journal of Thermal Sciences*, vol. 76, pp. 225–234, 2014.

[39] D. Deng, D. jie Liang, Y. Tang, J. Peng, X. dong Han, and M. Pan, "Evaluation of capillary performance of sintered porous wicks for loop heat pipe," *Experimental Thermal and Fluid Science*, vol. 50, pp. 1–9, 2013.

[40] J. Choi, W. Sano, W. Zhang, Y. Yuan, Y. Lee, and D.-A. Borca-Tasciuc, "Experimental investigation on sintered porous wicks for miniature loop heat pipe applications," *Experimental Thermal and Fluid Science*, vol. 51, pp. 271–278, 2013.

[41] J. J. Jasper, "The Surface Tension of Pure Liquid Compounds," *Journal of Physical and Chemical Reference Data*, vol. 1, pp. 841–1010, 10 2009.

[42] C. Busse, "Theory of the ultimate heat transfer limit of cylindrical heat pipes," *International Journal of Heat and Mass Transfer*, vol. 16, no. 1, pp. 169–186, 1973.

[43] S. Saygan, *Modeling Guided Heat Pipe Design Methodology and Experimental Validation for Flat Grooved Heat Pipes*. Phd thesis, Middle East Technical University, February 2021.

[44] B. Derebaşı, "Assessment of the effect of vapor flow on the thermal performance of a flat grooved heat pipe," Master's thesis, Middle East Technical University, June 2023.

[45] G. Gökçe, C. Kurt, G. Odabaşı, Z. Dursunkaya, and B. Çetin, "Comprehensive three-dimensional hydrodynamic and thermal modeling of steady-state operation of a flat grooved heat pipe," *International Journal of Multiphase Flow*, vol. 160, p. 104370, 2023.

[46] D. A. Nield and A. Bejan, *Convection in porous media*. Springer International Publishing, 2018.

[47] O. Rahli, L. Tadrist, M. Miscevic, and R. Santini, "Fluid Flow Through Randomly Packed Monodisperse Fibers: The Kozeny-Carman Parameter Analysis," *Journal of Fluids Engineering*, vol. 119, pp. 188–192, 03 1997.